High-Energy Electromagnetic Conversion Processes in Intense Magnetic Fields

THOMAS ERBER

Department of Physics, Illinois Institute of Technology, Chicago, Illinois

General characteristics of magnetic bremsstrahlung (synchrotron radiation) are derived on the basis of calculations utilizing exact relativistic matrix elements. The spectral and total energy losses may be described by compact expressions incorporating radiative and quantum corrections. Comparisons of the relative efficacy of matter and magnetic fields as bremsstrahlung radiators indicate that even under relatively conservative conditions the natural conversion rates associated with the magnetic process (i.e., 9.6×10^3 BeV/mm) tends to favor this type of conversion over ordinary bremsstrahlung.

Discussions of a similar scope—including detailed calculations, and comparisons with the corresponding processes in material media—are also carried out for magnetic pair production, direct and indirect trident cascades, and magnetic photon splitting.

Circumstances peculiar to a class of external field radiative processes involving cooperative vacuum polarization corrections are illustrated by a discussion of magnetic Čerenkov radiation.

1. INTRODUCTION

Electromagnetic conversion processes such as bremsstrahlung, pair production, and photon splitting may be catalyzed by the presence of external magnetic fields in essentially the same way as they may be catalyzed by the presence of external electric fields. In fact, from a theoretical point of view, the only significant distinction between these two kinds of processes arises from the circumstance that the symmetry between electric and magnetic vacuum polarization corrections is disturbed by the apparent absence of magnetic monopoles. A simple consequence of this asymmetry is the stability of arbitrarily strong uniform magnetic fields against spontaneous pair conversion as contrasted with the "Klein catastrophe" which is manifested in the corresponding electric case [B1]. Practically speaking however electromagnetic conversion processes occurring in external electric fields are far more familiar since the intense Coulomb fields surrounding atomic nuclei provide a readily accessible means for experimentally studying these transformations—notably bremsstrahlung and pair production. In contrast the only magnetic conversion process which has received any detailed attention to date is synchrotron radiation—or more precisely, magnetic bremsstrahlung—which may be observed at relatively low field intensities, and which is of some technical importance in connection with the design of accelerators.

Just as in the corresponding Coulomb case, magnetically induced conversion processes generally require both high-field strengths and high energies. This is essentially due to the fact that the transition probabilities are principally governed by a single parameter Υ defined by

$$\Upsilon\equiv(E/mc^2)(H/H_{\rm cr}), \tag{1.1}$$

where E is an energy characteristic of the process, e.g., the bombarding energy, H is the ambient magnetic field strength, mc^2 is the electron rest mass, and the quantity

$$H_{\rm cr}\equiv m^2c^3/e\hbar=4.414\times10^{13}\ \text{G}, \tag{1.1a}$$

denotes the natural quantum mechanical measure of magnetic field strength. The transition probabilities are generally increasing functions of Υ (in the range $\Upsilon\lesssim1$) and therefore significant conversion rates require both high energies and very intense magnetic fields.[1] In order to fix the relevant orders of magnitude it is instructive to refer to the early calculations of magnetic bremsstrahlung carried out in connection with betatron and synchrotron design [e.g., I1, B2]: These estimates were based on energy requirements principally in the 0.1- to 1.0-BeV range, and presumed magnetic steering field capabilities of the order of 5 to 15 kG. In keeping with these constraints, the calculations were based on Υ factors of the order of 10^{-7}; and, in view of the Υ^2 dependence of the bremsstrahlung matrix elements, led to the prediction of relatively feeble radiation rates. However it was already appreciated at this early stage that much greater bremsstrahlung rates, as well as a variety of other electromagnetic conversion processes, e.g., pair production and photon splitting, would become accessible if larger values of Υ could be achieved.

In this respect the experimental situation has altered appreciably: Various technical developments in the intervening years have resulted in drastic upward shifts of the attainable ranges of Υ. In particular, high-energy particle accelerators either committed, de-

[1] This relationship has some similarities to the link between high magnetic fields and cryogenics: The appropriate factor in this case is the Langevin parameter $\mathfrak{L}=\mu H/kT$. In cases where μ may be identified with the Bohr magneton, this can be rewritten as the product of two dimensionless factors, viz., $\mathfrak{L}=(mc^2/kT)(H/H_{\rm cr})$. As is well known, appreciable cooperative effects require values of $\mathfrak{L}$ approaching unity, and this clearly indicates the advantage of combining low temperatures and high fields. The analogy with the Υ parameter defined by Eq. (1.1) is evident.

signed, or planned have made it plausible to consider characteristic conversion energies of the order of 20 to 800 BeV; and the introduction of explosive flux compression techniques ("pulse-imploders") has boosted realizable magnetic field strengths to the 5- to 25-MG range.[2] Taken together, these figures imply Υ values in excess of 10^{-2}, or a total increase of five orders of magnitude over the older working estimates. Under these conditions it becomes possible to consider the extension of measurements of familiar effects such as magnetic bremsstrahlung to previously inaccessible ranges. It also becomes feasible to enhance external field radiative and quantum corrections to the point where they may be detectable as perturbations of familiar effects. And finally, the prospect of observing qualitatively new effects such as electrodynamic strong coupling modifications and vacuum polarization Čerenkov radiation moves closer to realization.[3]

In view of these developments it seems appropriate to review in some detail a number of the principal features of high-energy–high-field electromagnetic conversion processes, and to provide some tentative estimates of the technical requirements which will play a role in eventual experimental programs. The specific processes considered in the present review include: (a) magnetic bremsstrahlung [Sec. 2]; (b) magnetic pair production [Sec. 3]; (c) direct and indirect trident cascades [Sec. 4]; (d) photon splitting and magnetic Čerenkov radiation [Sec. 5]. As indicated previously, a number of related high-field–low-energy processes have already been considered elsewhere [E1, E2]. Most of the key points of the present survey are summarized in the following paragraphs:

(*a*) *Magnetic bremsstrahlung.* This process, under its more familiar name, "synchrotron radiation," is usually associated with direct microwave and optical emission from the circulating particle beams in high-energy accelerators.[4] In this context, magnetic bremsstrahlung is generally considered to be a low-energy phenomenon. Nevertheless, the intrinsic conversion rates (R_0) available with this process are of the order of 9.6×10^3 BeV/mm. The essential point is that under customary circumstances the value of Υ^2 is about 10^{-14}, and therefore the total emission rate—which is proportional to $R_0\Upsilon^2$—corresponds to comparatively insignificant radiative losses. For larger values of Υ however magnetic bremsstrahlung becomes more appreciable, and in fact under the conditions

$$(E/mc^2)\,(H/H_{\rm cr})^2\sim10^{-9}, \qquad (1.2)$$

the total radiation rate begins to compete favorably with the ordinary (Coulomb) bremsstrahlung conversion efficiency of solid copper. The magnetic bremsstrahlung spectrum has a peak in the vicinity of $E[3\Upsilon/(2+3\Upsilon)]$, and this provides some fiducial characteristics for energy calibration, as well as additional flexibility in the selective enhancement of radiation.

The bremsstrahlung calculations discussed in Sec. 2 are based on exact matrix elements utilizing the relativistic Dirac wave functions for uniform magnetic fields. It is therefore possible to treat relativistic and quantum effects with some confidence. One consequence is that previous conjectures [S1, N1] regarding the special significance of relativistic effects in enhancing quantum corrections have been confirmed in numerical detail. Experimentally, these effects are manifested in a reduction of the photon emission into portions of the spectrum above the normal bremsstrahlung peak. Values of Υ of the order of 10^{-2} are sufficient to demonstrate the onset of these quantum corrections [E7].

A practically unique feature of high-energy magnetic bremsstrahlung is the possibility of investigating electrodynamic strong coupling modifications. These effects become important when the forces of radiation reaction ($\mathbf{F}_R$) become comparable in magnitude to the Lorentz forces ($\mathbf{F}_L$) which ordinarily control the particle motion [E4]. Quantitatively this condition may be expressed in the form

$$|\,\mathbf{F}_R\,|/|\,\mathbf{F}_L\,|=\tfrac{1}{200}(H/H_{\rm cr})\,(E/mc^2)^2\rightarrow1; \qquad (1.3)$$

which implies experimental arrangements roughly on par with those required for the observation of quantum effects, i.e., $\Upsilon\sim10^{-2}$. By means of suitable variations of the experimental conditions it is in fact possible to study strong radiative corrections for magnetic bremsstrahlung with minimal interference from quantum mechanical effects. In this sense a nontrivial separation of these effects is feasible. The strong coupling features appear when one attempts to include these large radiative corrections in the usual quantum mechanical description: Simple perturbation theory then is no longer adequate, and the exact propagators must incorporate radiative modifications in addition to those already accounted for in the relativistic bound state Green's functions [e.g., K1, K2]. In contrast to other types of high-energy scattering experiments, non-electromagnetic strong interaction effects in this case remain isolated in higher-order vacuum polarization loops.

(*b*) *Magnetic pair production.* This process has not yet been observed experimentally. Although the minimum energy requirements are rather modest, i.e.,

[2] The technical basis for explosive flux compression [F1, F2, C1, E11, S10] is a conversion of chemical energy to magnetic field energy. The energy density of high explosives (circa 10^3 g-cal/cm^3) is roughly comparable to the energy densities of megagauss fields. Ultimately, higher field intensities may be achieved with pulse-imploders driven by nonconventional explosives.

[3] There are also a number of high-field low-energy effects of related interest. These depend on dispersive properties of magnetic vacuum polarization and generally involve experimental conditions of a completely different kind. These effects have been discussed in some detail in references [E1, E2, E3].

[4] These may be galaxies.

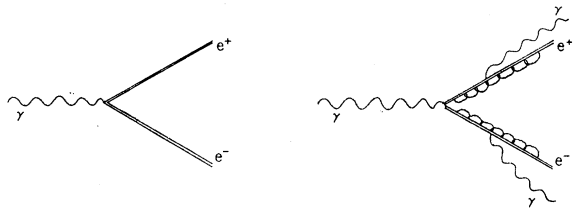

FIG. 1. (a) Pair production in a moderately strong field. The double lines denote the binding effects. (b) Pair production in a strong field. The bound propagators are modified by virtual photon (radiation reaction) loops.

$E/mc^2 \sim 2$, practical considerations place the actual threshold at

$$\Upsilon \gtrsim 10^{-1}, \tag{1.4}$$

which is technically a much more severe demand. Inasmuch as magnetic pair production is so closely linked to electric pair production there would seem to be little theoretical interest in studying its properties. Nevertheless there are certain questions of principle that may be more suitably explored with quasi-uniform magnetic fields than with spatially limited nuclear Coulomb fields. The basic concern is again with the influence of large external-field radiative corrections on the transition amplitudes for electromagnetic conversion processes (compare Fig. 1): Suppose for instance that magnetic pair production occurred at sufficiently high energies and in fields intense enough so that the effective threshold inequality (1.4) were satisfied. Then in almost all foreseeable circumstances at least one of the emerging particles would receive sufficient energy to place it well up near the strong radiation reaction limit given in (1.3). Experimentally this implies that the particle would itself become the source of intense secondary bremsstrahlung. Due to the strong radiation reaction the corresponding particle propagator would then have to include modifications over and above those already accounted for in relativistic and binding effects [T1, D1]. In this respect the situation parallels that already discussed in connection with magnetic bremsstrahlung. The new feature that makes an appearance in magnetic pair conversion is that the production vertex itself should in principle be calculated with this modified propagator. It is entirely possible that a self-consistent calculation utilizing nonperturbative techniques would yield results differing significantly from those implied by the estimates leading to (1.4). These types of strong coupling problems arising in connection with high-energy–high-field pair conversion calculations are very similar to those encountered in estimates of magnetic monopole production [M1, A1].

Some estimates for magnetic pair production are given in Sec. 3. In the absence of tractable nonperturbative techniques, the calculations have been optimized by employing the most accurate relativistic bound state propagators presently available. The final results should at least be adequate for preliminary experimental orientation.

Under conditions approximating (1.4), magnetic pair production becomes competitive with ordinary pair production in matter. For slightly larger values of Υ magnetic pair production in fact tends to become the dominant process. Basically the advantage lies with the magnetic fields because both the electric and magnetic conversion amplitudes approach an upper limit, i.e., saturate, as Υ increases past unity.[5] At very high energies the over-all transition rates are then limited by the total field volumes available for the conversions. In material media, the presence of bound electrons in the vicinity of nuclei places an effective upper limit on the Coulomb field volumes, and this leads to the well known screening limits on pair production. These equivalent Coulomb volumes are roughly of the order of (Avogadro's number) × (Compton wavelength)^3, or approximately 10^{-8} cm^3. As a consequence even very modest magnetic field volumes (of suitable intensity) can become competitive pair converters. This line of argument is of course not limited to pair production: in general under extreme conditions the combined influence of amplitude saturation and (Coulomb) volume limitations tends to favor magnetically induced conversion processes over the corresponding electric conversion processes.

The progressive saturation of Coulomb pair production, and related processes, at very high energies also has the practical consequence that the cross sections gradually become more insensitive to energy variations. This leads to difficulties in establishing reliable energy scales—particularly in the range above 10^{12} eV where cascade shower estimates are currently almost the only means for gauging the orders of magnitude of pertinent energies. These problems can in principle be overcome by taking advantage of the "tunability" available in adjusting the value of Υ for various magnetic conversion processes. As a specific illustration let us consider magnetic pair production where good energy calibrations can be achieved by choosing Υ to be in the range $\Upsilon \gtrsim \frac{1}{3}$. The total transition rates in this case depend principally on the rapidly varying factor

$$\exp\{-\tfrac{8}{3}[(E/mc^2)(H/H_{cr})]^{-1}\},$$

and it is evident that H may be chosen appropriately so as to bring the desired energy variations into this most sensitive range.

---

[5] More precisely, in the case of the magnetic scattering amplitudes, there is a leveling off and a subsequent decrease as Υ increases past unity. In the electric case the situation is completely analogous if one makes the replacement $\Upsilon \to \Upsilon\mathcal{E} \equiv (E/mc^2)(\mathcal{E}/\mathcal{E}_{cr})$ in the corresponding scattering amplitudes. In this case $\mathcal{E}$ denotes ambient electric field strength, and $\mathcal{E}_{cr} = m^2c^3/e\hbar = 1.323 \times 10^{16}$ V/cm. The relationship between the saturation of the scattering amplitudes and vacuum polarization effects has been discussed in detail in reference [E5].

(*c*) *Trident cascades.* The characteristic lengths associated with electromagnetic conversion processes are all of the order of a Compton wavelength ($\approx 3.85\times10^{-11}$ cm). Accordingly, magnetic fields spanning volumes even as small as a cubic millimeter appear to be of practically infinite extent in comparison with the individual conversion vertices. If conditions are adjusted so that the transition probabilities are not vanishingly small, one would then expect that the individual conversion events would rapidly multiply into cascade showers.[6] A crucial step in the initial growth and development of these showers is the occurrence of trident conversions, i.e., the processes

$$e^{\pm}+H\rightarrow e^{\pm}+\gamma+H\rightarrow e^{\pm}+e^{+}+e^{-}+H, \qquad (1.5)$$

where H represents the external magnetic field, and the intermediate photons may be either real or virtual. Estimates of the relevant transition amplitudes (Sec. 4) bear out the expectation that under extreme conditions, i.e., $\Upsilon\gtrsim\frac{1}{10}$, these trident cascades do in fact become an important component of the total magnetic attenuation.

(*d-1*) *Photon splitting.* A number of the usual selection rules of quantum electrodynamics are subject to modifications when external fields are present. One illustration of this is provided by photon splitting, or photon coalescence, which is ordinarily forbidden by Furry's theorem [F3; see also Fig. 2]. This process has not yet been observed experimentally, although in the particular case of Coulomb fields the cross sections are not impractically minute. Significant conversion rates for the corresponding magnetic process of course require extreme conditions, i.e., Υ values of the order of 0.02; but experimentally one has the advantage that competing processes such as double Compton scattering from atomic electrons may in principle be eliminated. Estimates and comparisons of magnetic and Coulomb photon splitting rates are summarized in Sec. 5.

(*d-2*) *Magnetic Čerenkov radiation.* Beyond the strong coupling modifications associated with extreme radiation reaction conditions [cf. (1.3)], there lies the possibility of cooperative radiative corrections arising from collective excitations of (external field) vacuum polarization loops. One effect of this type which has already been discussed on a number of previous occasions [e.g., E2, E3] is vacuum polarization Čerenkov radiation. Phenomenologically this effect is completely analogous to ordinary Čerenkov emission: Electromagnetic radiation propagating across a magnetic field in a direction perpendicular to the lines of flux will travel with a phase velocity less than the phase velocity of light in vacuum [T1, K1, K2]. Consequently charged particles with sufficiently high energies can traverse these fields with velocities exceeding the ambient light velocity, and may be expected to dissipate some of their energy through Čerenkov emission. Estimates based on phenomenological quantum electrodynamics [J1] yield a threshold for this effect of the order of $\Upsilon\gtrsim 60$. Since radiation reaction corrections are very important under these conditions these results are however liable to considerable modification. Semiquantitative estimates of the expected orders of magnitude—taking into account interference from magnetic bremsstrahlung—are discussed in Sec. 5.

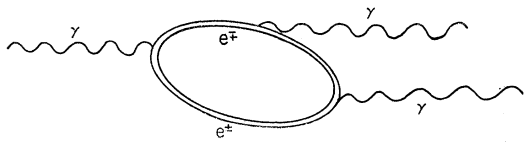

FIG. 2. Photon splitting in a strong field. One of the intermediate particles in a vacuum polarization loop emits a photon.

2. MAGNETIC BREMSSTRAHLUNG

A. Spectral Distribution and Total Energy Dissipation

Quantum mechanical calculations of magnetic bremsstrahlung are usually carried out within the framework of a bound state formalism, i.e., the Furry representation [F4]. The transition probabilities in this case lead to radiation rates rather than to cross sections. It is convenient to idealize the calculation by assuming that the entire process takes place in a uniform magnetic field (H) which is of infinite extent. The initial and final electron states (ψ_{e^-}) may then be represented as superpositions of bound state eigenfunctions derived from the Dirac Hamiltonian for a uniform magnetic field. ([J2], and further references cited therein.) These eigenfunctions can be conveniently classified according to their energy (E) and spin along the magnetic field direction (σ_H) in a suitable diagonal representation indexed with the corresponding quantum numbers n and s. The eigenvalue equation relating these quantities is given by

$$E=\pm mc^2[1+(H/H_{cr})(2n+s+1)]^{1/2};$$
$$n=0, 1, \cdots; \; s=\pm1. \qquad (2.1a)$$

There is an additional degree of freedom which represents the arbitrariness of spatial position in a plane perpendicular to the field direction. This indeterminacy gives rise to an infinite (energy) degeneracy with respect to the location of the orbit centers (r_0). The corresponding quantum number (l) may then be obtained from the eigenvalue condition

$$r_0^2\psi_{e^-}=\{(2l+1)(H_{cr}/H)\lambda\!\!\!^{-}_c{}^2\}\psi_{e^-}. \qquad l=1, 2, \cdots; \qquad (2.1b)$$

which exhibits the imprecision in the values of r_0^2. [As usual, $\lambda\!\!\!^{-}_c=\hbar/mc$; and the critical field is given by

[6] In view of the tremendous energy degradation of the individual shower components, this may be considered a "gedanken" device for shielding against ultrahigh-energy particles.

(1.1a).] Motion in a direction parallel to the magnetic field may be eliminated from the problem through a tacit transformation to a "center of drift" system.

With all these provisos, the normalized electron wave functions corresponding to states of definite energy and polarization may be written as

$$\psi_{e^-}=\sum_l \mid n, s, l\rangle; \tag{2.2}$$

where the explicit analytical forms are given in [J2]. The transition probability for magnetic bremsstrahlung, in simplest approximation, then may be computed by methods of ordinary first-order perturbation theory, viz.

$$W=2\pi(\alpha/\nu)$$
$$\times \sum_{ss'll'n'\epsilon} \mid \langle n', s', l' \mid \boldsymbol{\alpha}\cdot\boldsymbol{\epsilon} \exp(-i\mathbf{k}\cdot\mathbf{r}) \mid n, s, l\rangle \mid^2, \tag{2.3}$$

where $\nu=c \mid \mathbf{k} \mid /2\pi$ denotes the frequency of the emitted photon, and all the other symbols have their customary meaning (e.g., [K3]).

Of the nine operations indicated in (2.3), seven may be carried out by relatively straightforward methods: The summations and averages over the polarization ϵ and the spin indices s,s' are easily performed with the help of standard reductions from Dirac algebra. The n' summation is also immediate since this merely involves a projection of all the final-state components consistent with energy conservation. The spatial integrations—which include Laguerre functions arising from (2.2)—lead to standard hypergeometric functions. The technical difficulties enter at the next stage when one attempts to carry out the l, l' summations. These indices now appear as parameters in hypergeometric functions and at present there are no known closed forms for the requisite sums. This situation has some resemblance to the "azimuthal" quantum number summation problem in the corresponding Coulomb case (e.g., [E6]), and can be dealt with by analogous methods. The essential device that is required is an appropriate asymptotic simplification of the hypergeometric functions. In the present instance this is tantamount to specializing all the electromagnetic conversion processes to the extreme relativistic range. Specifically, *here and in all the succeeding calculations*, it is assumed that the experimental conditions are consistent with the inequalities

$$E/mc^2\gg 1, \quad \text{and} \quad (E-h\nu)/mc^2\gg 1, \tag{2.4}$$

where E now represents the *initial* electron energy, and $h\nu$ is the energy of the emitted photon.[7]

[7] The asymptotic expansion of the hypergeometric functions with respect to the parameters also requires the auxiliary condition $(h\nu/mc^2)^2\gg H/H_{cr}$, which ostensibly eliminates very soft photon conversion processes. In the bremsstrahlung case one can however *a posteriori* extend the final results [compare the Eqs. (2.10) and (2.11) of the text] down to the lower limit of the corresponding classical treatment [S2], viz., $h\nu/mc^2\gg(mc^2/E)(H/H_{cr})$. The assumption $H\leqq H_{cr}$ is also implicit in most of the computations (compare [T1]).

This part of the magnetic bremsstrahlung calculation was first explicitly carried through by N. P. Klepikov [K4]. His final result for the spectral distribution of the radiation emitted per unit distance may be written in the form:

$$I(E, h\nu, H)=\frac{3\alpha}{\pi^2}\frac{mc^2}{\lambda\!\!\!^{-}_c}\frac{\Upsilon}{(2+3\Upsilon)^2}\frac{y^2}{E}\mathfrak{M}(y, \Upsilon), \tag{2.5a}$$

where

$$\mathfrak{M}(y, \Upsilon)=\sum_{i=1}^{3}\mathfrak{M}_i(h\nu/E)\mathfrak{J}_i(y, \Upsilon), \tag{2.5b}$$

and

$$\mathfrak{M}_1(h\nu/E)=1+(1-h\nu/E)^{-2},$$
$$\mathfrak{M}_2(h\nu/E)=2/(1-h\nu/E), \tag{2.5c}$$
$$\mathfrak{M}_3(h\nu/E)=\left[\frac{h\nu/E}{1-h\nu/E}\right]^2;$$

furthermore

$$\mathfrak{J}_1(y, \Upsilon)=\int_0^\infty dx \cosh^5 x\, K^2_{2/3}\left[\frac{y}{2+3\Upsilon(1-y)}\cosh^3 x\right],$$

$$\mathfrak{J}_2(y, \Upsilon)=\int_0^\infty dx \cosh^3 x \sinh^2 x$$
$$\times K^2_{1/3}\left[\frac{y}{2+3\Upsilon(1-y)}\cosh^3 x\right], \tag{2.5d}$$

$$\mathfrak{J}_3(y, \Upsilon)=\int_0^\infty dx \cosh^5 x\, K^2_{1/3}\left[\frac{y}{2+3\Upsilon(1-y)}\cosh^3 x\right].$$

As in the preceding [compare (1.1)], the parameter Υ is defined by

$$\Upsilon=(E/mc^2)(H/H_{cr}). \tag{2.5e}$$

The K's appearing in the integrands of (2.5d) are modified Bessel functions conforming to Watson's conventions [W1]. The new notation

$$y=h\nu/h\nu_{cr}, \qquad h\nu_{cr}=E[3\Upsilon/(2+3\Upsilon)], \tag{2.5f}$$

has been introduced for convenience in characterizing the spectral distribution. (*Note*: $0\leq h\nu\leq E$ corresponds to $0\leq y\leq 1+2/3\Upsilon$.) As usual we write $\alpha=e^2/\hbar c$ for the fine structure constant.

The general behavior of the spectral function $I(E, h\nu, H)$ with respect to variations of the individual parameters of physical interest is rather complex. The situation can however be simplified considerably by taking advantage of the convenient circumstance that with the single additional restriction

$$h\nu\ll E, \tag{2.6}$$

the entire complex of analytical expressions (2.5a–d) may be reduced to a concise form which turns out to

be substantially identical to that derived from the corresponding classical problem.

We begin by expanding the $\mathfrak{M}_i$'s to first order in $h\nu/E$:

$$\begin{aligned}\mathfrak{M}_1(h\nu/E)&\cong 2[1+(h\nu/E)],\\ \mathfrak{M}_2(h\nu/E)&\cong 2[1+(h\nu/E)],\\ \mathfrak{M}_3(h\nu/E)&\cong \mathcal{O}(h\nu/E)^2\to 0.\end{aligned} \tag{2.7}$$

As a consequence of the elementary inequality

$$\partial K_\nu(z)/\partial\nu>0, \qquad \text{for } \nu>0,\ z>0; \tag{2.8a}$$

one may also show that

$$\mathcal{J}_1(y,\Upsilon)\geq\mathcal{J}_3(y,\Upsilon); \tag{2.8b}$$

and this leads to the rigorous upper bound

$$\frac{\mathfrak{M}_3(h\nu/E)\,\mathcal{J}_3(y,\Upsilon)}{\mathfrak{M}_1(h\nu/E)\,\mathcal{J}_1(y,\Upsilon)}\leq(h\nu/E)^2. \tag{2.8c}$$

To first order in $h\nu/E$, the $\mathfrak{M}$-representation (2.5b) may then be contracted to the single term

$$\begin{aligned}\mathfrak{M}(y,\Upsilon)\cong 2(1+h\nu/E)&\\ \times\int_0^\infty dx\,\Big\{&\cosh^5 x\,K^2_{2/3}\Big[\frac{y}{2+3\Upsilon(1-y)}\cosh^3 x\Big]\\ &+\cosh^3 x\sinh^2 x\,K^2_{1/3}\Big[\frac{y}{2+3\Upsilon(1-y)}\cosh^3 x\Big]\Big\}.\end{aligned} \tag{2.8d}$$

The essential step of the entire reduction now follows from the identity

$$\begin{aligned}\int_0^\infty dx\{&\cosh^5 x\,K^2_{2/3}(\zeta\cosh^3 x)\\ &+\cosh^3 x\sinh^2 x\,K^2_{1/3}(\zeta\cosh^3 x)\}\\ &=\frac{\pi}{2\sqrt{3}}\zeta^{-1}\int_{2\zeta}^\infty dx\,K_{5/3}(x), \qquad \zeta>0,\end{aligned} \tag{2.8e}$$

which is proved in Appendix 1. This permits the further simplification of (2.8d) to

$$\mathfrak{M}(y,\Upsilon)=\frac{\pi}{\sqrt{3}}(1+h\nu/E)\zeta^{-1}\int_{2\zeta}^\infty dx\,K_{5/3}(x), \tag{2.8f}$$

where

$$\begin{aligned}\zeta\equiv\frac{y}{2+3\Upsilon(1-y)}&=\frac{y}{(2+3\Upsilon)(1-h\nu/E)}\\ &\cong(3\Upsilon)^{-1}\frac{h\nu}{E}\Big(1+\frac{h\nu}{E}\Big);\end{aligned} \tag{2.8g}$$

the last approximation following from (2.6).

It is now convenient to introduce the auxiliary (bremsstrahlung) function

$$\kappa(z)\equiv z\int_z^\infty dx\,K_{5/3}(x), \tag{2.9}$$

corresponding to the incomplete Bessel function integrals appearing in (2.8e, f). This leads to a very compact final expression for the bremsstrahlung spectral distribution:

$$I(E,h\nu,H)=(\sqrt{3}\alpha/2\pi)(mc^2/\lambda\!\!\!^{-}_c)(\Upsilon/E)(1-h\nu/E)\kappa(2\zeta), \tag{2.10}$$

where all the notations and hypotheses are as specified in the equations (2.1b) to (2.9) of the preceding. The corresponding classical relativistic result [S2, S3, A2] may be put into the form[8]

$$I(E,h\nu,H)=\frac{\sqrt{3}\alpha}{2\pi}\frac{mc^2}{\lambda\!\!\!^{-}_c}\frac{\Upsilon}{E}\kappa\Big(\frac{2}{3\Upsilon}\frac{h\nu}{E}\Big). \tag{2.11}$$

It is clear that the classical and quantum mechanical expressions are almost identical. The most important distinctions arise from the fact that Υ is *not* necessarily restricted by the condition $\Upsilon\gg1$ in (2.10); and also that the argument of κ in the quantum mechanical form is modified by the factor $(1+h\nu/E)$. These points are discussed in some detail in Sec. 2B.

Various properties of the bremsstrahlung function $\kappa(z)$ are derived in Appendix 2. For reference we note the limiting forms

$$\kappa(z)\begin{cases}\nearrow\ 2.149z^{1/3}, & z\ll1\\ \searrow\ 1.253z^{1/2}e^{-z}, & z\gg1.\end{cases} \tag{2.12}$$

The function is displayed graphically in Fig. 3; numerical values are given in Table I.

These formulas may be simplified still further in circumstances where the additional restriction

$$(h\nu/E)(1+h\nu/E)\ll\Upsilon, \tag{2.13}$$

is applicable. In view of (2.6) this is in fact satisfied identically in the quantum mechanical regime $\Upsilon\gtrsim1$. From (2.10) and (2.12) we then find

$$I(E,h\nu,H)=0.517\alpha\frac{mc^2}{\lambda\!\!\!^{-}_c}\frac{\Upsilon^{2/3}}{E}\Big(\frac{h\nu}{E}\Big)^{1/3}\Big(1-\frac{2}{3}\frac{h\nu}{E}\Big), \tag{2.14}$$

[8] The usual forms of this equation are easily recovered by shifting from an energy to a frequency scale ($I\to\hbar I$); and converting the quantum mechanical critical field to the corresponding classical expression [L1], e.g., $\alpha^{-1}H_{qr}=m^2c^4/e^3=H_{cr}$(classical).

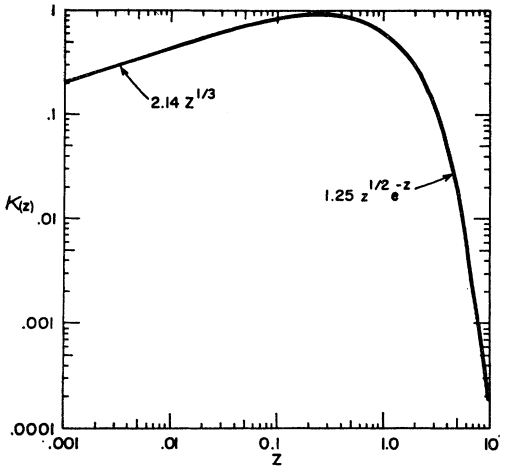

FIG. 3. Graph of the bremsstrahlung function;

$$\kappa(z)=z\int_z^\infty dx K_{5/3}(x).$$

where

$$\alpha(mc^2/\lambda_c)=9.657\times10^3\ \text{BeV/mm} \qquad (2.14a)$$

is the intrinsic rate of magnetic bremsstrahlung.

It is also useful to have an explicit formula for the total radiation per unit distance into the spectral region between $h\nu_1$ and $h\nu_2$. This follows immediately from (2.14);

$$\frac{\mathcal{E}(h\nu_1, h\nu_2)}{\Delta x}=4.99\times10^3\,\Upsilon^{2/3}\int_{h\nu_1/E}^{h\nu_2/E} dx\, x^{1/3}\,(1-\tfrac{2}{3}x)\ \text{BeV/mm}. \qquad (2.15)$$

In particular, for the integral spectrum we obtain

$$\mathcal{E}(0, h\nu)/\Delta x \cong 3.75\times10^3\,\Upsilon^{2/3}\,(h\nu/E)^{4/3}\ \text{BeV/mm}. \qquad (2.16)$$

A rough measure of the value of Υ in a given experimental situation may be derived from the position of the maximum intensity of the bremsstrahlung spectrum. This is a consequence of inverting (2.5f) to give

$$\Upsilon=\frac{2}{3}\frac{h\nu_{cr}/E}{1-h\nu_{cr}/E}, \qquad (2.17)$$

and identifying $h\nu_{cr}$ with the bremsstrahlung peak [compare (2.8g)]. In general this maximum increases with increasing values of Υ; and ultimately for $\Upsilon>\frac{2}{3}$, the magnitude of $h\nu_{cr}$ tends towards the top end of the spectrum, i.e., $h\nu_{cr}\to E$. Further information on E and H may in principle be obtained by combining measurements of the differential spectrum, such as (2.15), with determinations of the bremsstrahlung peak.

The total energy dissipation per unit distance may be obtained from the basic expression (2.5a) by an integration over all frequencies. The exact analytical form of this result has been given by Klepikov [K4]. It is convenient to write this as

$$\Delta\mathcal{E}(\Upsilon)/\Delta x=\tfrac{2}{3}\alpha(mc^2/\lambda_c)\,g(\Upsilon), \qquad (2.18)$$

where

$$g(\Upsilon)=\begin{cases}\Upsilon^2(1-5.953\Upsilon), & \Upsilon\ll1; \quad (2.18a)\\ 0.5563\Upsilon^{2/3}, & \Upsilon\gg1. \quad (2.18b)\end{cases}$$

A graph of the exact function is given in Fig. 4.

Both limiting cases corresponding to $\Upsilon\gtrless1$ may be obtained directly from (2.10). In particular it is easy to check that the expression (2.16), with the ratio $h\nu/E\to1$, lies within 5% of the exact quantum mechanical limit (2.18b). The leading term of the small Υ-expansion (2.18a) of course coincides with the classical result.

B. Quantum Corrections and Radiation Reaction

Under conditions of high momentum transfer it is expected that quantum effects will appreciably influence the characteristics of magnetic bremsstrahlung. The classical theory may therefore be considered reliable only under circumstances where the ratio of the photon to the particle momentum is essentially neg-

TABLE I. Numerical values for the function $\kappa(z)$.

z	$\kappa(z)$	z	$\kappa(z)$
0.001	0.213	1.0	0.651
0.01	0.445		
0.02	0.547	2	0.300
0.03	0.614		
0.04	0.663	4	0.053(+0, −0.002)
0.05	0.701		
0.06	0.733	5	0.0214(+0, −0.0008)
0.07	0.760		
0.08	0.782	6	0.00845(+0, −0.00008)
0.09	0.801		
0.1	0.818	7	0.00338
0.2	0.903		
0.3	0.924	8	0.00129
0.4	0.905		
0.5	0.871	9	0.00049
0.6	0.831	10	0.00019
0.7	0.788		
0.8	0.742		
0.9	0.696		

ligible. A rough criterion for this is

$$\frac{h\nu_{cr}/c}{E/c}\sim\Upsilon\ll 1. \tag{2.19}$$

At extremely high energies however relativistic effects may enhance the influence of quantum corrections: Various features of high-energy bremsstrahlung depend sensitively on the velocity increment $c-v\sim(c/2)(mc^2/E)^2$, and in the ultrarelativistic region this is diminished to magnitudes comparable with the quantum fluctuations. More refined wave packet arguments [S1] have in fact indicated that the inequality (2.19) ought to be replaced by the stricter condition

$$\Upsilon^{1/2}\ll 1; \tag{2.19a}$$

and it has been conjectured [N1] that quantum modifications may actually be manifested under even more conservative conditions. The observation of these effects is of course favored by circumstances sensitive to the relativistic enhancement. It will appear that the shape of the upper portion of the bremsstrahlung spectrum exhibits significant quantum corrections even for Υ values as low as 10^{-2}.

These points may be checked in quantitative detail with the aid of the classical and quantum mechanical expressions (2.11) and (2.10). The total radiated energy emitted (per unit distance) into portions of the bremsstrahlung spectrum between $h\nu_1$ and $h\nu_2$ is given by

$$\frac{\Delta\mathcal{E}(h\nu_1, h\nu_2)}{\Delta x}=\int_{h\nu_1}^{h\nu_2} d(h\nu)I(E, h\nu, H). \tag{2.20}$$

In the classical case the explicit form of this result is

$$\frac{\Delta\mathcal{E}^{cl}(h\nu_1, h\nu_2)}{\Delta x}=\frac{3^{3/2}\alpha}{4\pi}\frac{mc^2}{\lambda\!\!\!^{-}_c}\Upsilon^2\int_{y_1}^{y_2} dy\,\kappa(y), \tag{2.20a}$$

where[9] $y=(2/3\Upsilon)(h\nu/E)$. The corresponding quantum mechanical expression is

$$\frac{\Delta\mathcal{E}^{QM}(h\nu_1, h\nu_2)}{\Delta x}=\frac{3^{3/2}\alpha}{4\pi}\frac{mc^2}{\lambda\!\!\!^{-}_c}\Upsilon^2\int_{y_1}^{y_2} dy\left(1-\frac{3\Upsilon}{2}y\right)\kappa\left(y+\frac{3\Upsilon}{2}y^2\right). \tag{2.20b}$$

Although y itself is not necessarily a small quantity, we shall assume that $\Upsilon y^2\ll 1$, and then introduce the series

[9] This is consistent with the previous notation (2.5f) in cases where $\Upsilon\ll 1$.

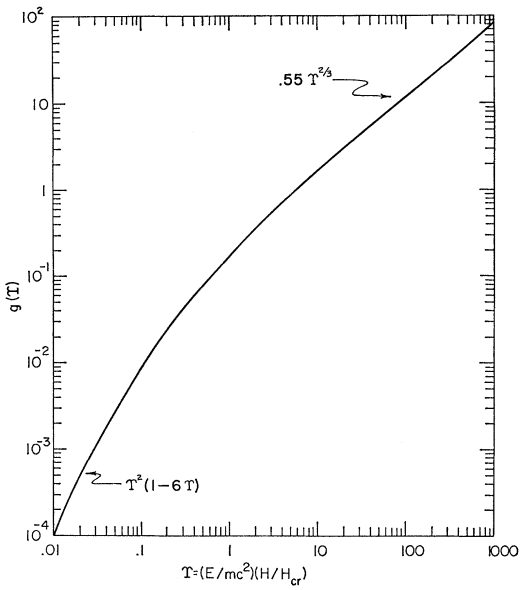

FIG. 4. Graph of the auxiliary function $g(\Upsilon)$ [cf. (2.18)].

expansion

$$\kappa[y+(3\Upsilon/2)y^2]\approx\kappa(y)+(3\Upsilon/2)y^2\,\kappa'(y)+\mathcal{O}(\Upsilon^2y^4). \tag{2.21}$$

Then

$$\int_{y_1}^{y_2} dy[1-(3\Upsilon/2)y)\,\kappa(y+(3\Upsilon/2)y^2]\approx\int_{y_1}^{y_2} dy\,\kappa(y) +\tfrac{3}{2}\Upsilon\left\{y_2^2\,\kappa(y_2)-y_1^2\,\kappa(y_1)-3\int_{y_1}^{y_2} dy\,y\,\kappa(y)\right\}. \tag{2.22}$$

Evidently the region $0.3<y_1,\ 5\lesssim y_2$ is of greatest interest. However since the function $\kappa(y)$ is already very small in the range $y>5$, the y_2 dependence will in fact not be too crucial. [For the same reason even the limit $y_2\to\infty$ does not clash with the initial assumption (2.21).] The quantum corrections to the upper portion of the bremsstrahlung spectrum then may be written in the compact form

$$\frac{\Delta\mathcal{E}^{cl}(h\nu,\infty)-\Delta\mathcal{E}^{QM}(h\nu,\infty)}{\Delta\mathcal{E}^{cl}(h\nu,\infty)}=\Upsilon\,f\left(\frac{2}{3\Upsilon}\frac{h\nu}{E}\right), \tag{2.23a}$$

where

$$f(y)=\frac{3}{2}\left(\left[y^2\,\kappa(y)+3\int_y^\infty dz\,z\,\kappa(z)\right]\Big/\int_y^\infty dz\,\kappa(z)\right). \tag{2.23b}$$

For $f(y)$ we have the representative values:

y	1	2	3	
$f(y)$	11	20	35.	(2.23c)

It is then apparent that even if the parameter Υ is assumed to be as small as 10^{-2}, the relative energy depletion in the spectral region above $h\nu/E\sim 0.004$ will be of the order of 35%. Analytically this enhancement is due to the considerable variation in magnitude of $\kappa(2\zeta)$ in a region expecially sensitive to small shifts of the argument. As is evident from (2.8g) the shift in this case results from the combination of a quantum effect, i.e., the replacement $1\rightarrow 1+h\nu/E$ in Eq. (2.10) with the relativistic enhancement due to the factor $(2/3\Upsilon)$.

Momentum transfer to the radiation field is also of importance in connection with a number of effects due to radiation reaction. Within the framework of the classical theory it is usually assumed that the dynamical characteristics of magnetic bremsstrahlung may be derived from the equation [E4]

$$\mathbf{F}_L+\mathbf{F}_R=\mathbf{P}, \tag{2.24}$$

where $\mathbf{F}_L$ is the Lorentz force exerted by the magnetic field and $\mathbf{F}_R$ represents the force of radiation reaction. It is well known that there are a number of unresolved theoretical difficulties associated with the derivation and application of this equation. In most cases of practical interest however these problems are of no concern since the experimental conditions imply the inequality

$$|\,\mathbf{F}_R\,|\ll|\,\mathbf{F}_L\,|, \tag{2.25}$$

and this permits the calculation of all necessary radiative corrections from (2.24) by simple perturbation methods. These approximations lead to analytically well defined results a d have the virtue of automatically avoiding the "runaway solutions" and other unpleasant features inherent in the exact form of (2.24). In the special case of magnetic bremsstrahlung it is however feasible to create experimental conditions for which the inequality (2.25) is no longer valid. The rigorous consequence of the "exact" radiation reaction theory may then be checked in a nontrivial way.

We again consider intense magnetic fields and bremsstrahlung in the ultrarelativistic limit: The Lorentz force in this case is given by

$$\mathbf{F}_L\sim e\hat{v}\times\mathbf{H}, \tag{2.26a}$$

where $\hat{v}$ is the unit velocity vector associated with the particle motion. The corresponding reaction force may then be estimated in an essentially model-independent way from the momentum transfer to the radiation field. Since most of the bremsstrahlung is emitted into a forward cone of half-angle $\sim mc^2/E(\ll 1)$, the transverse momentum components may be neglected and $\mathbf{F}_R$ obtained directly from (2.18), i.e.,

$$\mathbf{F}_R\sim-\frac{d(E/c)}{dt}\hat{v}=-\frac{2}{3}\alpha\frac{mc^2}{\lambda\!\!\!^{-}_c}g(\Upsilon)\hat{v}. \tag{2.26b}$$

From an experimental point of view the most favored situations involve the condition $\Upsilon\ll 1$; and this implies the further simplification $g(\Upsilon)\rightarrow\Upsilon^2$ [compare (2.18a)]. In these cases the momentum transfer ratio is explicitly given by

$$|\,\mathbf{F}_R\,|/|\,\mathbf{F}_L\,|\sim\tfrac{2}{3}\alpha(H/H_{cr})(E/mc^2)^2. \tag{2.27a}$$

From this expression it is obvious that the equality

$$|\,\mathbf{F}_R\,|\sim|\,\mathbf{F}_L\,|, \tag{2.27b}$$

can indeed be satisfied with a variety of plausible experimental arrangements. Some representative choices for E and H are:

E (BeV)	20	40	200	300	1000	
H (gauss)	6.0×10^6	1.5×10^6	6.0×10^4	2.6×10^4	2.4×10^3	
Υ	5.4×10^{-3}	2.7×10^{-3}	5.4×10^{-4}	3.5×10^{-4}	1.1×10^{-5}	. (2.28)

(See also Table IV.) Under these conditions one would expect appreciable changes in the dynamics and the radiation characteristics of magnetic bremsstrahlung.

It is important to recognize that the equality (2.27b) does not necessarily imply a breakdown of classical electrodynamics. This is presumably a Lorentz-covariant theory and the criteria limiting its domain of validity ought to have a Lorentz-invariant significance. This obviously is not the case for (2.27a) which is merely the ratio of the magnitudes of 3-vectors. For this reason a number of authors have proposed that the value assumed by (2.27a) in the particle rest system—evidently an invariant—be identified as the actual limit for the internal consistency of the theory

[P1, L1, E4]. Elementary transformations of this ratio yield

$$(|\mathbf{F}_R|/|\mathbf{F}_L|)_{\text{rest}} \sim \tfrac{2}{3}\alpha(E/mc^2)(H/H_{\text{cr}}), \qquad (2.29)$$

where E and H retain their meaning as energy and field strength measured with respect to the laboratory system. It is apparent that the invariant criterion $(|\mathbf{F}_R| \ll |\mathbf{F}_L|)_{\text{rest}}$ is far more conservative than (2.25).

This line of argument, apart from its theoretical significance, has the practical merit of suggesting a reasonable approach to the computation of radiation reaction effects even under conditions violating the inequality (2.25): A comparison of the two ratios (2.29) and (2.27a) indicates that Lorentz transformations to the rest system generally tend to diminish the importance of radiation reaction. This implies that perturbation methods may be legitimately applied in the rest system under circumstances where this is not directly feasible in the laboratory system. Specifically in cases where the equality (2.27b) applies but the ratio (2.29) still remains small, radiation reaction effects may be evaluated by perturbation theory in the rest frame, and the results then transformed back to the laboratory system. These perturbed solutions may of course differ considerably from the initial solutions. The net result of the radiation reaction feedback will be to alter the normal spectral distribution [i.e., (2.11)] of the bremsstrahlung.

A special feature of high-energy magnetic bremsstrahlung is that the spectral perturbations due to quantum mechanical effects and radiation reaction corrections can in principle be distinguished from each other. This possibility is a consequence of the differences in the respective threshold criteria, i.e. (2.23a, b) and (2.27a, b). Theoretically this is an extremely interesting situation since in all other known cases (see [E4]) quantum effects intervene well before conditions reach the point where radiative corrections become important. This is reflected in the usual theoretical sequence in which quantum mechanical descriptions are first substituted for the classical formulations; and only afterwards—if necessary—supplemented by quantum mechanical perturbations which correct for the radiative effects. The Lamb shift and the Schwinger correction [S4] are well-known illustrations of the success of this approach both for low- and high-energy radiation reaction effects. In the magnetic bremsstrahlung case however it is evident that experimental conditions can be adjusted so that at the point where quantum corrections become important strong radiation reaction effects already prevail. This corresponds to an inadequacy of the relativistic electron propagators [K2, T1] even in lowest approximation. A proper description would obviously have to incorporate radiative corrections *ab initio*. In this sense high-energy bremsstrahlung becomes a problem in quantum electrodynamics involving *strong coupling but without strong interactions.*

C. Comparison of Bremsstrahlung in Matter and Magnetic Fields

In the energy region above 10 BeV, and for magnetic field strengths exceeding 1 MG, electron bremsstrahlung in magnetic fields begins to compete favorably with electron bremsstrahlung in material media. In this section we present a detailed comparison of the differential and total energy dissipation rates for the two processes. The basic expressions for magnetic bremsstrahlung can be taken over from the preceding work. The corresponding formulas for material media may be obtained from the compilation of Koch and Motz [K6]. It is convenient to restrict the energies to the range

$$1600/Z \ll E/mc^2 \lesssim 10^6, \qquad (2.30)$$

where Z is atomic number. Ionization losses at low energies may then be ignored, and theoretical complications peculiar to super-high energies (cf. Sec. 2D) will not vitiate the comparisons.

The best estimates currently available for the spectral intensity of very-high-energy electron bremsstrahlung in materials characterized by density ρ, atomic weight A, and atomic number Z lead to the expression

$$I(h\nu, Z) = \tfrac{8}{3}\alpha N_0 \lambda\!\!\!^{-}_c{}^2 h(Z), \qquad (2.31a)$$

where N_0 is Avogadro's number, $\lambda\!\!\!^{-}_c$ is the Compton wavelength, and $\alpha = \text{"1/137"}$. Screening effects and Coulomb corrections are included in the auxiliary function $h(Z)$ which is given by

$$h(Z) = 6(\rho/A)(\alpha Z)^2 [\ln(183/Z^{1/3}) + 0.083 - 1.20(\alpha Z)^2 \{1 - 0.86(\alpha Z)^2\}]. \qquad (2.31b)$$

This form of $I(h\nu, Z)$ is a good first approximation for the spectral bremsstrahlung per unit distance appropriate in the extreme relativistic region. It omits a weak dependence on photon energy and cannot be relied upon at all near the bremsstrahlung tip, $h\nu \sim E$. (Both Coulomb and magnetic bremsstrahlung cross-section estimates in this region are still rather uncertain.) For purposes of comparison we shall use (2.31a) to represent the effects of bremsstrahlung in material media, and the expression (2.10) for the corresponding magnetic spectrum, viz.

$$I(E, h\nu, H) = \frac{\sqrt{3}\alpha}{2\pi} \frac{mc^2}{\lambda\!\!\!^{-}_c} \frac{\Upsilon}{E} \left(1 - \frac{h\nu}{E}\right) \kappa(2\xi). \qquad (2.32)$$

The total bremsstrahlung energy dissipation per unit distance in material media is given by

$$\frac{\Delta \mathcal{E}(Z)}{\Delta x} = \int^E d(h\nu) I(h\nu, Z); \qquad (2.33)$$

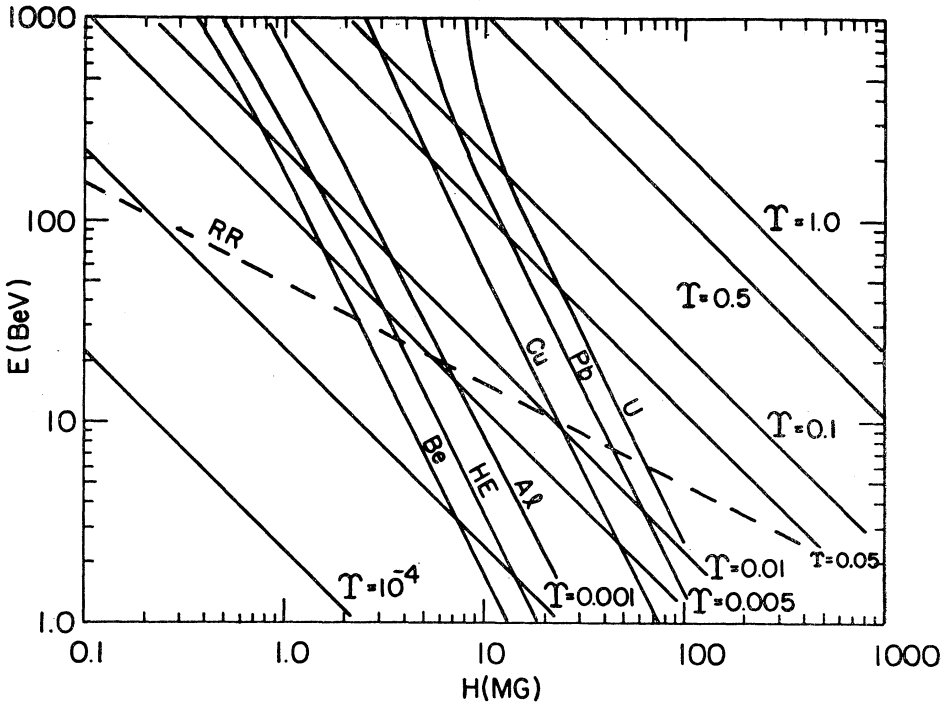

FIG. 5. Summary of the total bremsstrahlung break-even conditions (2.38) for various materials. The regions to the right of the curves labeled Be, HE, Al, etc. correspond to experimental conditions favoring magnetic bremsstrahlung. As an illustration we note that at 300 BeV the minimum magnetic field required to enhance magnetic bremsstrahlung over ordinary bremsstrahlung in high explosives is 1 MG (≡megagauss).

The curves below $\Upsilon=0.01$ represent the equations

$$E_{\mathrm{BeV}}H^2_{\mathrm{MG}}=3.44\times10^4\,h(z); \qquad \text{[cf. (2.39)]}.$$

The remaining portions correspond to solutions of the implicit conditions

$$g(\Upsilon)=6.77\times10^{-5}E_{\mathrm{BeV}}\,h(z); \qquad \text{[cf. Fig. 4]}.$$

The line "RR" marks the onset of the strong radiation reaction regime (2.27a, b).

and the best current estimate for this quantity is

$$\Delta\mathcal{E}(Z)/\Delta x=\tfrac{2}{3}\alpha N_0\lambda\!\!\!^{-}_c{}^2\,E\,h(Z). \qquad (2.34)$$

The corresponding magnetic expression [compare (2.18)] is

$$\Delta\mathcal{E}(\Upsilon)/\Delta x=\tfrac{2}{3}\alpha(mc^2/\lambda\!\!\!^{-}_c)g(\Upsilon). \qquad (2.35)$$

Since we are principally interested in assessing the comparative magnitudes of these quantities it is convenient to introduce two ratios: the total energy dissipation ratio

$$R_B=\frac{\Delta\mathcal{E}(\Upsilon)/\Delta x}{\Delta\mathcal{E}(Z)/\Delta x}=2.89\times10^7\,\frac{mc^2}{E}\,\frac{g(\Upsilon)}{h(Z)}\,; \qquad (2.36)$$

and the spectral intensity ratio

$$R_B(h\nu)=\frac{I(E,h\nu,H)}{I(h\nu,Z)}=0.89\times10^7\left(1-\frac{h\nu}{E}\right)\frac{H}{H_{\mathrm{cr}}}\,\frac{\kappa(2\zeta)}{h(Z)}. \qquad (2.37)$$

The large numerical factor ($\sim10^7$) which appears in both of these expressions represents the total "Compton volume" $N_0\lambda\!\!\!^{-}_c{}^3(=3.465\times10^{-10})$ which provides the natural scale for Coulomb-induced conversion processes in bulk matter under fully screened conditions. The small value of this quantity is one of the factors favoring the magnetically catalyzed conversions.

A fairly quick way of becoming familiar with the various experimental possibilities covered by R_B and $R_B(h\nu)$ is to consider first the break-even point for the total radiation rates. The corresponding experimental conditions are then implicitly determined by the equation

$$R_B=1. \qquad (2.38)$$

In cases where $\Upsilon\ll\frac{1}{6}$, this is equivalent to the simple relation

$$(E/mc^2)(H/H_{\mathrm{cr}})^2=3.46\times10^{-8}\,h(Z). \qquad (2.39)$$

Under more extreme conditions the exact form of (2.36) must be used. Representative values for $h(Z)$ are given in Table II. The experimental conditions required to reach break-even for a number of materials are summarized graphically on Fig. 5. For convenience,

TABLE II. Representative values for $h(Z)$.

	Beryllium	Air	High explosive	Aluminum	Copper	Lead	Uranium
Z	4	~7	~8	13	29	82	92
A	9	~14	~16	27	63	204	238
ρ	1.84	1.25×10^{-3}	1.7	2.70	8.89	11.00	18.7
$h(Z)$	5.00×10^{-3}	6.44×10^{-6}	9.89×10^{-3}	0.024	0.156	0.409	0.734

curves of constant Υ are also indicated on the figure (compare Table III).

Figure 5 shows that for magnetic fields in the 1–10 MG range and energies above 10-BeV magnetic bremsstrahlung does indeed begin to compete favorably with bremsstrahlung in material media. In the range 100–1000 BeV—which is of interest in connection with projected high energy accelerators—even fields as modest as 1 MG (i.e., pulsed coil configurations or magnetically driven Cnare imploders) can be considered as practical bremsstrahlung converters. These trends become increasingly pronounced at still higher magnetic field strengths. Some of the estimates shown on Fig. 5 must be regarded with caution since the comparisons involving curves above the RR-line are subject to considerable radiation reaction corrections.[10]

A comparison of the spectral intensities of Coulomb and magnetic bremsstrahlung is given in Fig. 6. The curves illustrate the special case of a 20-BeV electron accelerator with a magnetic target adjusted to a field strength of 3 MG. This normalizes the total magnetic bremsstrahlung to the same level as the total ordinary (Coulomb) bremsstrahlung in beryllium, cf. the break-even criteria (2.38), (2.39). It is clear from the figure that under these conditions the low energy end of the spectrum will be completely dominated by magnetic bremsstrahlung. The energy $h\nu_1$ indicated on this graph is defined by the relation

$$h\nu_1 = 1.5E\Upsilon; \qquad (2.40)$$

and serves as a convenient marker of the upper end of the most intense part of the magnetic bremsstrahlung spectrum. The quantity $h\nu_2(\equiv 5h\nu_1)$ which also appears on the figure corresponds roughly to the upper energy limit of the useful portion of the spectrum; beyond this point the intensity dwindles very rapidly. Entries listing values of $h\nu_1$ and $h\nu_2$ corresponding to various experimental conditions are given in Table IV.

Figure 6 also exhibits the situation for a 1000-BeV device: In this case the beryllium target bremsstrahlung extends up towards 1000 BeV, but in virtue of the saturation of the transition amplitudes the absolute magnitude of the intensity does not increase beyond the level reached at 20 BeV. The peak of the corresponding magnetic spectrum ($H=3$ MG) is shifted to approximately 70 BeV, with a useful intensity excess extending up to about 700 BeV. Beyond this point present bremsstrahlung estimates become too uncertain to warrant detailed comparisons. The R_B ratio (2.36) appropriate to this case is of the order of 40.

Table IV contains a summary of the results of similar analyses for a variety of energies, field strengths, and target materials. The general trend of these comparisons supports the view that higher energies favor the magnetic interactions.

D. Bremsstrahlung Comparisons (continued)

There are a number of ultrahigh-energy effects which lead to modifications of the simple bremsstrahlung com-

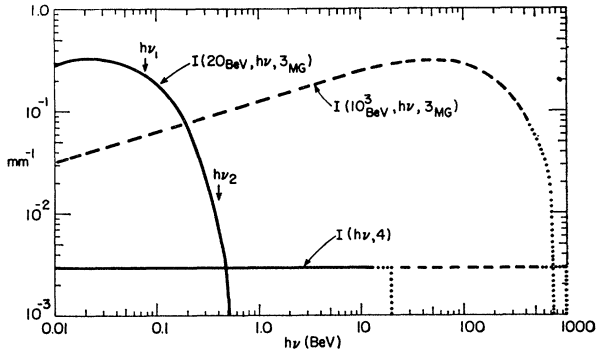

FIG. 6. Comparison of electron bremsstrahlung in beryllium and magnetic fields. In practical units

$$I(E, h\nu, H) \quad 0.12H_{MG}\,\kappa\left(\frac{2}{3\Upsilon}\frac{h\nu}{E}\right)\text{mm}^{-1}, \qquad \text{[cf. (2.32)]};$$

and

$$I(h\nu, Z) \simeq 0.58h(Z)\,\text{mm}^{-1}, \qquad \text{[cf. (2.31a)]}.$$

The actual radiation rates, in units of energy/mm, are given by $I(h\nu, Z)\Delta(h\nu)$ and $I(E, h\nu, H)\Delta(h\nu)$. The solid curves indicate the intensities for the conditions $E=20$ BeV and $H=3$ MG which have been adjusted to correspond to break-even, i.e., $R_B=1$ as in (2.38). The dashed curves represent the situation at $E=1000$ BeV with H remaining at 3 MG. The curve segments set off by ••• correspond to regions of theoretical uncertainty near the bremsstrahlung tip. For the definitions of $h\nu_1$ and $h\nu_2$, see (2.40) of the text.

[10] Present bremsstrahlung target materials are limited to total beam power loads of the order of 30 kW/cm² [M2]. It remains to be seen whether this limitation will favor magnetic targets in high-energy high-current devices.

TABLE III. Values of $\Upsilon=4.43\times10^{-5}\,E(\text{BeV})H(\text{MG})$.

E_{BeV}	H_{MG}									
	0.1	0.5	1.0	2.0	3.0	4.0	5.0	6.0	7.0	8.0
1000	4.4×10^{-3}	22×10^{-3}	44×10^{-3}	89×10^{-3}	13×10^{-2}	18×10^{-2}	22×10^{-2}	27×10^{-2}	31×10^{-2}	36×10^{-2}
900	4.0	20	40	80	12	16	20	24	28	32
800	3.6	18	36	71	11	14	18	21	25	28
700	3.1	16	31	62	9.3	12	16	19	22	25
600	2.7	13	27	53	8.0	11	13	16	19	21
500	2.2	11	22	44	6.7	8.9	11	13	16	18
400	1.8	8.9	18	36	5.3	7.1	8.9	11	12	14
300	1.3	6.7	13	27	4.0	5.3	6.7	8.0	9.3	11
200	0.89	4.4	8.9	18	2.7	3.6	4.4	5.3	6.2	7.1
100	0.44	2.2	4.4	8.8	1.3	1.8	2.2	2.7	3.1	3.6
90	0.40	2.0	4.0	8.0	1.2	1.6	2.0	2.4	2.8	3.2
80	0.36	1.8	3.6	7.1	1.1	1.4	1.8	2.1	2.5	2.8
70	0.31	1.6	3.1	6.2	0.93	1.2	1.6	1.9	2.2	2.5
60	0.27	1.3	2.7	5.3	0.80	1.1	1.3	1.6	1.9	2.1
50	0.22	1.1	2.2	4.4	0.67	0.89	1.1	1.3	1.6	1.8
40	0.18	0.89	1.8	3.6	0.53	0.71	0.89	1.1	1.2	1.4
30	0.13	0.67	1.3	2.7	0.40	0.53	0.67	0.80	0.93	1.1
20	8.9×10^{-5}	0.44	0.89	1.8	0.27	0.36	0.44	0.53	0.62	0.71
10	4.4	0.22	0.44	0.88	0.13	0.18	0.22	0.27	0.31	0.36
6	2.7	0.13	0.27	0.53	8.0×10^{-4}	0.11	0.13	0.16	0.19	0.21
1	4.4×10^{-6}	2.2×10^{-5}	4.4×10^{-5}	8.9×10^{-5}	1.3	1.8×10^{-4}	2.2×10^{-4}	2.7×10^{-4}	3.1×10^{-4}	3.6×10^{-4}

E_{BeV}	H_{MG}										
	9.0	10	20	30	40	50	60	70	80	90	100
1000	40×10^{-2}	44×10^{-2}	88×10^{-2}	1.3	1.8	2.2	2.7	3.1	3.6	4.0	4.4
900	36	40	80	1.2	1.6	2.0	2.4	2.8	3.2	3.6	4.0
800	32	36	71	1.1	1.4	1.8	2.1	2.5	2.8	3.2	3.6
				($\Upsilon=1$, $E=752$)							
700	28	31	62	0.93	1.2	1.6	1.9	2.2	2.5	2.8	3.1
600	24	27	53	0.80	1.1	1.3	1.6	1.9	2.1	2.4	2.7
500	20	22	44	0.67	0.89	1.1	1.3	1.6	1.8	2.0	2.2
400	16	18	36	0.53	0.71	0.89	1.1	1.2	1.4	1.6	1.8
300	12	13	27	0.40	0.53	0.67	0.80	0.93	1.1	1.2	1.3
											($\Upsilon=1$, $E=225$)
200	8.0	8.9	18	0.27	0.36	0.44	0.53	0.62	0.71	0.80	0.89
100	4.0	4.4	8.8	0.13	0.18	0.22	0.27	0.31	0.36	0.40	0.44
90	3.6	4.0	8.0	0.12	0.16	0.20	0.24	0.28	0.32	0.36	0.40
80	3.2	3.6	7.1	0.11	0.14	0.18	0.21	0.25	0.28	0.32	0.36
70	2.8	3.1	6.2	9.3×10^{-2}	0.12	0.16	0.19	0.22	0.25	0.28	0.31
60	2.4	2.7	5.3	8.0	0.11	0.13	0.16	0.19	0.21	0.24	0.27
50	2.0	2.2	4.4	6.7	8.9×10^{-2}	0.11	0.13	0.16	0.18	0.20	0.22
40	1.6	1.8	3.6	5.3	7.1	8.9×10^{-2}	0.11	0.12	0.14	0.16	0.18
30	1.2	1.3	2.7	4.0	5.3	6.7	8.0×10^{-2}	9.3×10^{-2}	0.11	0.12	0.13
20	0.80	0.89	1.8	2.7	3.6	4.4	5.3	6.2	7.1×10^{-2}	8.0×10^{-2}	8.9×10^{-2}
10	0.40	0.44	0.88	1.3	1.8	2.2	2.7	3.1	3.6	4.0	4.4
6	0.24	0.27	0.53	0.80	1.1	1.3	1.6	1.9	2.1	2.4	2.7
1	4.0×10^{-4}	4.4×10^{-4}	8.8×10^{-4}	0.13	0.18	0.22	0.27	0.31	0.36	0.40	0.44

TABLE IV. Summary of magnetic bremsstrahlung characteristics.

Accelerator energy	Material	Magnetic "break-even" field	Υ	Total energy dissipation	$h\nu_1$[d]	$R_B(h\nu_1)$	$h\nu_2$[d]	$R_B(h\nu_2)$
20 BeV	RR[a]	6.0 MG	5.3×10^{-3}	180 MeV/mm	160 MeV	...	...	...
	Be	3.0	2.7	45	79	79	400 MeV	2.5
	HE[b]	4.2	3.7	90	110	56	560	1.8
	Al	6.4	5.7	210	170	35	850	1.1
40 BeV	RR	1.5	2.7×10^{-3}	45	160	...	...	...
	Be	2.1	3.7	89	220	55	1.1 BeV	1.8
	HE	3.0	5.3	180	320	40	1.6	1.3
	Al	4.5	8.0	410	480	25	2.4	0.80
	Cu	10	18	2100	1100	8.6	5.4	0.27
300 BeV	RR	2.6×10^4 G	3.5×10^{-4}	0.77 MeV/mm	160 MeV	...	...	...
	Be	0.75 MG	1.0×10^{-2}	0.64 BeV/mm	4.5 BeV	20	23 BeV	0.63
	HE	0.98	1.3	1.1	5.9	13	29	0.42
	Al	1.5	2.0	2.6	9.0	8.2	45	0.26
	Cu	4.5	6.0	23	27	3.7	...[c]	...
	Pb	7.2	9.6	55	43	2.3	...	...
	U	11	14	96	60	1.9	...	...
1000 BeV	RR	2.4×10^3 G	1.1×10^{-4}	72 keV/mm	160 MeV	...	...	...
	Be	0.38 MG	0.017	2.2 BeV/mm	26 BeV	10.0	130 BeV	...
	HE	0.52	0.023	4.3	35	6.7	170	...
	Al	0.84	0.037	10	56	4.6	280	...
	Cu	2.5	0.11	68	170	2.1	...	...
	Pb	5.0	0.22	180	330	1.6	...	...
	U	7.9	0.35	320	525	...[c]	...	...

[a] RR refers to the radiation reaction condition (2.27a, b); compare Fig. 5.
[b] HE=high explosives (PBX or Composition "B").
[c] Entries omitted because the condition $h\nu \ll E$ is violated.
[d] For definitions of these energies see Eq. (2.40) and the subsequent remarks.

parisons considered in the previous section. In particular it has already been emphasized that magnetic bremsstrahlung under strong radiation reaction conditions, i.e., in the region above "RR" on Fig. 5, will exhibit deviations from the quantum mechanical results (2.32) and (2.35). There are similar corrections for ordinary bremsstrahlung which arise from coherent effects in condensed material media. Generally these effects introduce nontrivial frequency variations in the flat Bethe–Heitler spectrum (2.31a) and are responsible for reductions in the over-all radiative losses.

In the energy region of interest, i.e., 10–10^3 BeV, the most important of these coherent effects is the multiple scattering inhibition originally discussed by Landau and Pomeranchuk [L3, M3, M4, D2]. This originates in the relativistic amplification of the intrinsic coherence length associated with the bremsstrahlung scattering amplitude [S5]. At incident electron energies exceeding 10^8 eV this coherence length becomes comparable to interatomic distances and the bremsstrahlung conversion can no longer be idealized as occurring in the vicinity of a single nucleus.[11] In order to discuss this process quantitatively it is convenient to introduce several characteristic energies [G1, G2]:

$$E_l \simeq [200/h(Z)][\rho Z/A]^{1/2}\, mc^2; \tag{2.41}$$

$$E_0 \simeq 3.5\times10^6\, mc^2/h(Z); \qquad [\text{for } h(Z) \text{ see (2.31b)}] \tag{2.42}$$

$$h\nu_l \simeq \gamma E^{2/3}, \qquad \gamma = E_l^{4/3}/E_0; \tag{2.43}$$

$$h\nu_u \simeq E^2/E_0. \tag{2.44}$$

Multiple scattering corrections become important for incident electron energies above the threshold $E>E_l$. The bremsstrahlung region most strongly affected lies between the limits

$$\nu_l \lesssim \nu \lesssim \nu_u. \tag{2.45}$$

In this interval the Bethe–Heitler spectrum is modified by the inhibiting factor q as follows:

$$I(h\nu, Z) \rightarrow q(E, h\nu, Z)\, I(h\nu, Z),$$

where

$$q(E, h\nu, Z) \simeq [(2\times10^3)/E][h\nu\, mc^2/h(Z)]^{1/2}. \tag{2.46}$$

For example, $q(10^3$ BeV, 0.1 BeV, $4)\sim\frac{1}{5}$, which confirms that under certain conditions the reduction of the

[11] This coherence phenomenon is a direct relativistic counterpart to coherent multiple photon scattering [B3, B4].

TABLE V. Critical energies (eV).

	Beryllium	Air	High explosive	Aluminum	Copper	Lead	Uranium
E_l	1.8×10^{10}	3.9×10^{11}	9.2×10^{9}	4.7×10^{9}	1.3×10^{9}	5.1×10^{8}	3.6×10^{8}
E_0	3.5×10^{14}	2.7×10^{17}	1.8×10^{14}	7.3×10^{13}	1.1×10^{13}	4.3×10^{12}	2.4×10^{12}
γ	0.13	0.011	0.13	0.13	0.12	0.11	0.11

ordinary bremsstrahlung intensity may indeed be considerable. In the special case $E\to E_l$, and $\nu\to\nu_l$, it is easy to check that $q\to1$, so that the inhibition vanishes. In the opposite limit $\nu\to\nu_u$ (but $E>E_l$), the factor q on the left-hand side of (2.46) must be replaced by $q(1-q)^{-1/2}$, and one again finds $q\to1$. Under conditions corresponding to $E>E_l$, but $\nu<\nu_l$ (i.e., $h\nu\lesssim10^8$ eV), the expression (2.46) no longer applies and the Landau–Pomeranchuk spectrum goes into the Ter-Mikaeljan spectrum.[12] A number of related possibilities are discussed in reference [G1].

Values of the critical energies for a number of materials are summarized in Table V. This information is also given graphically on Fig. 7. For illustration the spectral regions exhibiting the multiple scattering reduction corresponding to the specific incident energy 10^3 BeV are indicated on the figure.

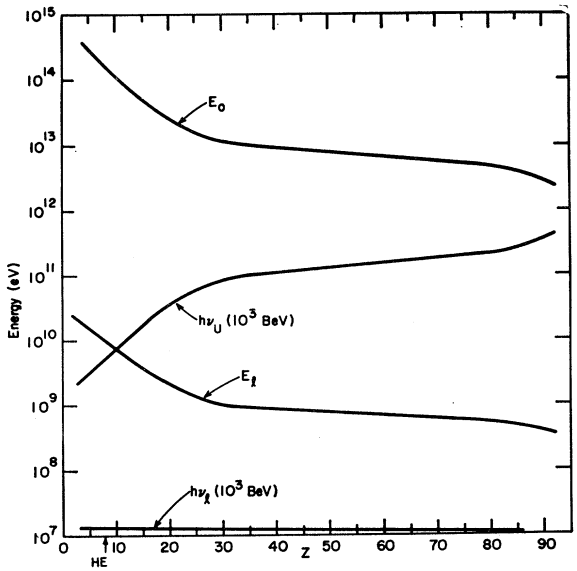

FIG. 7. Critical energies for coherent bremsstrahlung corrections. The curves $h\nu_l$ and $h\nu_u$ [compare (2.43) and (2.44)] mark the boundaries of the spectral regions which are damped by the Landau–Pomeranchuk effect corresponding to the special choice $E\sim10^3$ BeV.

[12] This refers to an additional reduction of low-energy bremsstrahlung emission due to the effects of the polarization of the medium [T2]. Several other effects of this type have been considered by Toptygin [T3] and Feinberg and Pomeranchuk [F5].

At this stage one could in principle return to Sec. 2C and undertake a revision of all the previously computed high-energy (i.e., $E>E_l$) bremsstrahlung comparisons to allow for the Landau–Pomeranchuk effect. However in view of the likely prospect of still further revisions which may eventually be required for radiation reaction and other coherent effects this does not seem advisable at present. It will be sufficient to illustrate the kinds of modifications that can be expected by considering one specific case: If we refer back to Fig. 6 we may easily obtain the values of the differential magnetic/Coulomb bremsstrahlung comparison factor $R_B(h\nu)$ appropriate to beryllium. Comparing with Fig. 7, it is evident that for incident energies $E\sim10^3$ BeV, the Landau–Pomeranchuk spectrum includes the special value $h\nu\sim0.1$ BeV. According to the preceding discussion the corresponding q-reduction for these specific conditions is $\sim\frac{1}{5}$. In this instance therefore the multiple scattering inhibition enhances the relative importance of magnetic bremsstrahlung by boosting the spectral ratio $R_B(0.1\text{ BeV})$ from 20 to 100.

Similar trends in the relative enhancement of magnetic bremsstrahlung can be discerned in connection with a number of other coherent effects.[13] For example the coherence length associated with the Landau–Pomeranchuk inhibition is approximately given by

$$l\simeq2\times10^3\,\lambda\!\!\!^{-}_c E\,[h\nu\times mc^2\times h(Z)]^{-1/2}. \qquad (2.47)$$

At very high energies this length can become comparable to the macroscopic target dimensions and the corresponding bremsstrahlung matrix elements will contain terms dependent on the surface configuration. In cases where these targets are "thin" relative to l, the bremsstrahlung dissipation may be expected to exhibit a saturation. For energies of the order of $10^5\,E_l$, self-absorption due to pair production begins to play a role and bremsstrahlung emission is damped still further.[14]

[13] Probable exceptions in this respect are corrections of the Frisch–Überall type [F6, U1].

[14] More precisely, we expect that the total bremsstrahlung losses will exhibit an energy dependence $\Delta\mathcal{E}/\Delta x\sim\mathcal{O}(E^{\frac{1}{2}})$, for $E_l\lesssim E\lesssim1.4\times10^5E_l$; and furthermore that $\Delta\mathcal{E}/\Delta x\sim\mathcal{O}(E^{-1})$, for $E\gtrsim1.4\times10^5E_l$ [G2]. In the absence of corresponding modifications for $g(\Upsilon)$, this implies that $R_B\to\infty$ for $E\to\infty$ [compare (2.36)].

There are some special circumstances in which the observation of the recoil electrons associated with (quasi-elastic) bremsstrahlung can be of practical interest. A particular example is the detection and calibration of transient magnetic fields trapped in the interior of explosive flux compressors [F1]. This type of experiment is based on the fact that explosive materials are relatively transparent to incident electrons with sufficiently high energy [compare Fig. 5]. In particular under conditions where $E>E_l$, electrons traverse high explosives with a mean deflection angle [per coherence length (2.47)] given approximately by

$$\theta_{\mathrm{HE}}\simeq\bar{q}^{-1/2}\, mc^2/E, \tag{2.48a}$$

where the factor $\bar{q}$, corresponding to the Landau–Pomeranchuk region, may be derived from (2.46).

On the other hand, a transverse magnetic field $H_\perp$ localized in a region of diameter d scatters such electrons through an angle

$$\theta_{H\perp}\simeq\frac{d}{\lambda\!\!\!^{-}_c}\frac{H_\perp}{H_{\mathrm{cr}}}\frac{mc^2}{E}\,. \tag{2.48b}$$

Experimental conditions can in fact be adjusted so that $\theta_{H\perp}\gg\theta_{\mathrm{HE}}$, and these large-angle deflections advantageously exploited for high-field studies.

3. PAIR PRODUCTION

A. General Remarks on Magnetic Field–Photon Interactions

Among the many different kinds of mechanism available for mediating magnetic field-photon interactions there are two particular processes which are closely linked through crossing symmetry and time reversal to the bremsstrahlung matrix elements discussed in the previous section.

One of these processes is inverse-bremsstrahlung [Fig. 8(a)], which for strongly bound initial states may be regarded as a direct analog of the atomic photoeffect. In the present context this type of conversion is relevant for experimental arrangements concerned with the generation of intense magnetic fields containing a plasma: This kind of system is essentially the equivalent of an n-electron "super-atom" capable of sustaining large momentum transfers during internal transitions. If such a magnetically stiffened plasma matrix (or plasma counter) is bombarded with high-energy photons it should in principle exhibit an enormous opacity in virtue of inverse-bremsstrahlung since the basic energy transfer rates are scaled by the same factors that appear in the direct process, i.e., $\alpha mc^2/\lambda\!\!\!^{-}_c\sim 10^4$ BeV/mm (2.14a). Some qualitative features of this type of conversion may be inferred from the magnetic Compton scattering calculations of Robl [R1]. More refined estimates are unfortunately not available at present.

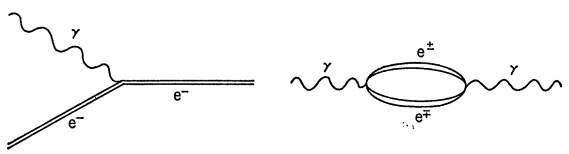

FIG. 8. (a) Feynman diagram for inverse-bremsstrahlung in a magnetic field. (b) Feynman diagram for a simple vacuum polarization loop.

The other photon interaction related to bremsstrahlung is pair production [Fig. 1(a)]. This process differs from bremsstrahlung in the important respect that although conservation laws do not forbid the interaction for photon energies above the threshold $h\nu\gtrsim 2mc^2$, the conversion rate is impractically small unless the condition $\frac{1}{2}(h\nu/mc^2)(H/H_{\mathrm{cr}})\equiv\chi\rightarrow 0.1$ is satisfied. This is a very severe requirement, and in fact magnetic pair production has not yet been observed experimentally. However once the parameter χ reaches the range $\chi\gtrsim 0.1$, the photon attenuation coefficient increases rapidly and magnetic pair production begins to dominate the corresponding process in matter. In principle strong magnetic fields are capable of degrading photons of arbitrarily high initial energy through direct pair production, as well as by means of other higher-order processes such as trident production, and electromagnetic shower development [e.g. Fig. 1(b)]. These points are discussed in quantitative detail in the following sections.

For purposes of computation it is convenient to order the magnetic field–photon conversion processes according to the powers of the coupling constant (α) which appear in the matrix elements. However just as in the case of the corresponding sequence of interactions associated with the Coulomb field, i.e., the photoeffect, Compton scattering, pair production, etc. a simple ordering according to powers of the coupling constant does not necessarily reflect the actual experimental importance of each process. A simple illustration of this is provided by magnetic vacuum polarization [Fig. 8(b)], which is a significant component in a number of physical effects including the reduction of the velocity of light in transverse magnetic fields, despite the fact that it is of second order in α and involves virtual pairs in the intermediate states. These types of vacuum polarization effects are essentially high-field–low-energy phenomena and can be observed under circumstances where lower-order processes such as pair production do not exist [E1, E2].

Returning to high-energy–high-field phenomena, we note that further examples of magnetic field–photon interactions include photon splitting [S6, E8] and photon coalescence [K7]. These are represented by the third-order bubble diagrams shown on Fig. 2. Under appropriate conditions magnetic photon splitting can actually dominate magnetic pair production. These problems are discussed in some detail in Sec. 5B.

B. Magnetic Pair Production

It is convenient to idealize the physical situation corresponding to magnetic pair production by considering the propagation of light across a uniform unbounded magnetic field in a direction perpendicular to the lines of flux. Since the magnetic field may absorb momentum, there is a nonvanishing probability that photons with sufficient energies ($h\nu \gtrsim 2mc^2$) will convert into electron–positron pairs. For a bound-state problem of this kind it is appropriate to express the conversion probability in terms of a photon attenuation coefficient $\alpha(\chi)$, which determines the actual number of pairs (n_{pairs}) created for a photon path length (d) in the magnetic field (H),

$$n_{\text{pairs}} = n_{\text{photons}} \{1 - \exp[-\alpha(\chi)\, d]\} \simeq n_{\text{photons}}\, \alpha(\chi)\, d. \tag{3.1}$$

The parameter $\chi \equiv \frac{1}{2}(h\nu/mc^2)(H/H_{\text{cr}})$ appearing in this expression is the essential factor governing the rate of pair conversion. It plays a role analogous to the parameter Υ in bremsstrahlung. The matrix element for this process, corresponding to the diagram of Fig. 1(a), leads to the expression

$$\alpha(\chi) = 2\pi(\alpha/\nu) \times \sum_{ss'll'nn'\epsilon} |\langle n', s', l' \mid \boldsymbol{\alpha}\cdot\boldsymbol{\epsilon} \exp(-ik\cdot r) \mid n, s, l\rangle|^2, \tag{3.2}$$

which is analogous to the bremsstrahlung form (2.3) except that now the "initial" spinor represents an outgoing positron. The explicit evaluation of this attenuation coefficient in the ultrarelativistic limit, neglecting all but the leading terms in $E(e^{\pm})/mc^2$, assuming $H \ll H_{\text{cr}}$, and disregarding various kinds of magnetic and electron–positron bound-state resonances [E2, G3, A3], has been described in detail on a number of previous occasions [R2, T1, K4]. The final results may be expressed in the form

$$\alpha(\chi) = \tfrac{1}{2}(\alpha/\lambda\!\!\!^{-}_c)(H/H_{\text{cr}})\, T(\chi), \tag{3.3a}$$

where the dimensionless auxiliary function $T(\chi)$ is given by

$$T(\chi) = \frac{4}{3\pi^2\chi^2}\int_0^\infty\!\!\int_0^\infty du\, dw \times \Big\{[2\cosh^2 w \cosh^5 u - \sinh^2 u \cosh^3 u] \times K^2_{1/3}\Big(\frac{2}{3\chi}\cosh^2 w \cosh^3 u\Big) + [2\cosh^2 w - 1] \times \cosh^5 u\, K^2_{2/3}\Big(\frac{2}{3\chi}\cosh^2 w \cosh^3 u\Big)\Big\}. \tag{3.3b}$$

The asymptotic properties of the modified Bessel functions appearing in this integral representation may be used to establish the limiting cases:

$$T(\chi) = \begin{cases} 0.46 \exp\{-4/(3\chi)\}, & \chi \ll 1; \\ 0.60\, \chi^{-1/3}, & \chi \gg 1. \end{cases} \tag{3.3c}$$

An excellent analytic approximation for $T(\chi)$ is given by the expression

$$T(\chi) \cong 0.16 \chi^{-1} K^2_{1/3}(2/3\chi). \tag{3.3d}$$

This function is graphed in Fig. 9; some representative values are listed in Table VI.

Equations (3.3a) and (3.3d) may be combined to give a concise expression for the photon attenuation coefficient,

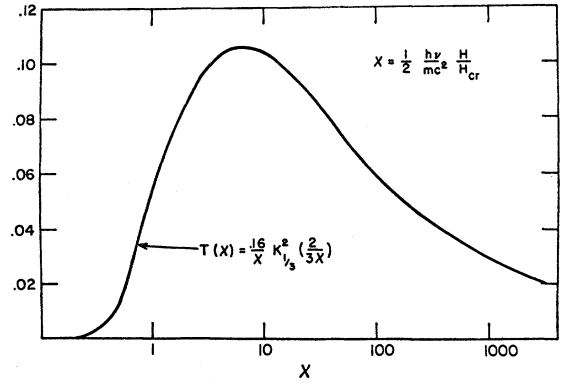

FIG. 9. The magnetic pair production function $T(\chi)$; compare (3.4a-d).

$$\alpha\left(\frac{1}{2}\frac{h\nu}{mc_2}\frac{H}{H_{\text{cr}}}\right) = 0.16\,\frac{\alpha}{\lambda\!\!\!^{-}_c}\frac{mc^2}{h\nu}\, K^2_{1/3}\left(\frac{4}{3}\frac{mc^2}{h\nu}\frac{H_{\text{cr}}}{H}\right). \tag{3.4}$$

This indicates clearly that the attenuation coefficient is not a symmetric function of the magnetic field strength and photon energy. In particular, considering H to be fixed, it is easy to verify that $\alpha(\chi)$ has a unique maximum with respect to variations of the photon energy which occurs at the point

$$h\nu_{\max}/mc^2 \simeq 12(H_{\text{cr}}/H); \tag{3.5}$$

and corresponds to Max $\{T(6)\} \sim 0.1$. On the other hand, regarding ν as fixed, it follows from (3.4) that the attenuation coefficient is a strictly increasing function of magnetic field strength. This implies that sufficiently intense magnetic fields are in principle completely efficient pair converters for photons of arbitrarily high energy. Comparing with (3.1) we see that this is equivalent to the condition $\alpha(\chi)\, d' \to 1$, or the

explicit criterion

$$H(\mathrm{MG})\, d'(\mathrm{mm}) \rightarrow 46. \tag{3.6a}$$

The associated photon energies are approximately bounded from below by

$$h\nu/mc^2 \gtrsim 6\times 10^6\, d'(\mathrm{mm}). \tag{3.6b}$$

This characteristic shielding distance (d') is still very much smaller than the radius of curvature (R) of the emergent photopairs. This follows immediately from the relation

$$R/d' \sim 10^3\, d'(\mathrm{mm}). \tag{3.6c}$$

C. Pair Production Comparisons

We now evaluate the relative efficacy of magnetic fields and material targets as pair converters. It is convenient to carry out these comparisons in terms of the respective attenuation coefficients. The pertinent result for magnetic fields is given by (3.3a). The best current estimate for the corresponding attenuation coefficient in material media, including both relativistic and Coulomb corrections, is given by the expression [D3]

$$\beta(Z) = \tfrac{14}{27}\,\alpha N_0 \lambda_c^2 \hat{h}(Z), \tag{3.7}$$

where

$$\hat{h}(Z) = h(Z) - 0.640(\rho/A)(\alpha Z)^2, \tag{3.7a}$$

and $h(Z)$ is the function defined in (2.31b). Since we are considering the ultrarelativistic case ($h\nu \gg mc^2$), the matrix elements leading to (3.7) have been evaluated in the fully screened limit and this results in an attenuation coefficient which is independent of the energy.

The condition for competition of pair production in matter and magnetic fields then is equivalent to

$$\alpha(\chi) \simeq \beta(Z);$$

TABLE VI. The magnetic pair production function $T(\chi)$.

χ	$T(\chi)$
0.2	2×10^{-4}
0.3	2.2×10^{-3}
0.4	6.6×10^{-3}
0.7	0.026
1.2	0.055
3.0	0.094
5.0	0.10
6.0	0.10
7.0	0.10
9.0	0.10
15	0.099
30	0.085

TABLE VII. Break-even points for pair production in material media and magnetic fields.[a]

Substance	Attenuation coefficient (mm^{-1})	Energy (BeV) 20	40	300	1000	10 000
Air	4×10^{-6}	200	100	15	5	...
Be	3×10^{-3}	300	160	30	10	2
Cu	0.1	...	300	50	20	5
Pb	0.3	...	320	70	30	8

[a] Table entries in megagauss (MG).

and inserting (3.3a) and (3.7), this leads to the requirement

$$(H/H_{\mathrm{cr}})\, T(\chi) \simeq 3.59\times 10^{-8}\, \hat{h}(Z). \tag{3.8}$$

Due to the high-energy saturation of pair production in material media it is clear that magnetic pair production will eventually dominate under sufficiently extreme conditions. The precise values of the photon energies and magnetic field strengths corresponding to the break-even point may be obtained by inverting the equality (3.8). Results for a number of representative cases are listed in Table VII and given graphically on Fig. 10.

The general trend of these figures indicates that magnetic pair production becomes a significant competitor for pair conversion in material media only in

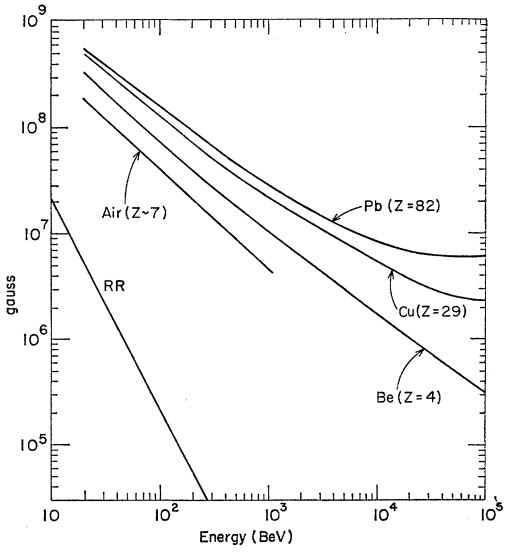

FIG. 10. Break-even curves for pair production in magnetic fields and various material media. The position of the "RR" line (2.27a, b) indicates that *all* of these curves lie in the strong radiation reaction region.

TABLE VIII. Minimum magnetic fields for break-even in pair production.

Element	Field (MG)	Energy (BeV)	Υ
Be	0.08	4×10^6	~14
Cu	2.4	1.3×10^5	~14
Pb	6.3	5×10^4	~14

the region $H\gtrsim 10$ MG, $h\nu\simeq 100$ BeV. The associated photon attenuation rates vary from moderate, i.e., 0.003 mm^{-1} corresponding to break-even for beryllium, to severe, i.e., 0.3 mm^{-1} corresponding to break-even for lead. In view of the comparisons with air it is however clear that the *existence* of magnetic pair production could in principle be demonstrated under experimentally less demanding conditions.

The absorption maximum discussed previously in connection with the attenuation coefficient (3.4) may also be utilized to find the *minimum* magnetic field strength compatible with the break-even condition (3.8). The corresponding photon energy may then be determined from equation (3.5). Some of these results are given in Table VIII. Evidently the energies associated with break-even for minimum magnetic fields are quite large. In view of the fact that the corresponding Υ values are greater than unity, these results should however be considered only as semiquantitative indications. As emphasized previously, magnetic pair production under these conditions can be expected to exhibit considerable modifications due to radiation reaction effects, and reliable methods for taking these into account are not available at present.

4. TRIDENT CASCADES

A. Trident Production by Virtual Photons

At very high energies and in intense magnetic fields the trident production process

$$e^{\pm}\rightarrow e^{\pm}+e^{+}+e^{-} \tag{4.1}$$

can become a significant element in the development of electromagnetic showers. The Feynman diagram for this process is shown on Fig. 11. The intermediate photon leading to the pair vertex may be either real or virtual; and in an exact calculation coherent contributions from both of these processes will appear in the transition amplitudes. We are however at present interested only in a preliminary quantitative orientation and interference effects arising from this source will be neglected. In the present section we estimate the virtual photon contribution to trident production on the basis of the Fermi–Weizsäcker–Williams (FWW) approximation. In the next section we evaluate the real photon contribution as a two step process involving bremsstrahlung and subsequent pair production. In the last section the relative conversion rates of these two processes are consolidated and compared with the corresponding rates of trident production in material media.

It is convenient to express the results of the trident production calculations directly in terms of the expected number of events per unit path length. Specifically for the virtual photon trident process we introduce the function $N_V^{(T)}(E, H)$ to represent the average number of events occurring during the passage of n electrons of energy E through a path length d in a transverse magnetic field H. This is given by

$$N_V^{(T)}(E,H)=nd\sum_{\nu}\mathfrak{N}(\nu)\alpha(\nu); \tag{4.2}$$

where $\mathfrak{N}(\nu)$ is the number of equivalent photons of frequency ν carried along by an electron, and $\alpha(\nu)$ is the absorption coefficient for pair production (3.3a). The Fourier resolution of the electron field then leads to the expression[15] [F7, W3, W4]

$$\mathfrak{N}(\nu)=(2/\pi)(\alpha/h\nu)W(h\nu/E)\,d(h\nu), \tag{4.3a}$$

where

$$W(\chi)=\chi K_0(\chi)K_1(\chi)-(\chi^2/2)[K_1^2(\chi)-K_0^2(\chi)]. \tag{4.3b}$$

Appropriate expansions of the modified Bessel functions in this expression yield the limiting cases

$$W(\chi)=\begin{cases}-\ln\chi, & \chi\ll 1;\\ (\pi/4)\,e^{-2\chi}, & \chi\gg 1.\end{cases} \tag{4.3c}$$

Since the pair production coefficient has a maximum in the vicinity of $h\nu\sim 12(H/H_{cr})mc^2$, it is clear from (4.3c) that trident conversion may be expected to increase logarithmically with energy. This is indeed confirmed by the details of the calculation. In order to obtain an explicit expression for the virtual photon trident conversion rate we substitute (4.3a) and (3.3a)

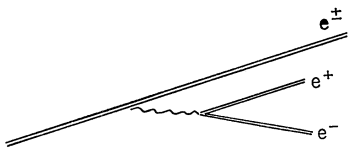

FIG. 11. Diagram for trident production in an external field.

[15] These estimates could in principle be improved with a covariant form of the Fermi–Weizsäcker–Williams approximation [B5].

into (4.2). After some rearrangement this can be written in the form

$$N_V^{(\Upsilon)}(E,H)=nd(0.32/\pi)(\alpha^2/\lambda\!\!\!^{-}_c)(H/H_{cr})\hat{\Omega}(\Upsilon), \quad (4.4)$$

where

$$\hat{\Omega}(\Upsilon)=\int_0^\infty du\, u^{-2}\, W(u/\Upsilon)K^2_{1/3}(4/3u). \quad (4.4a)$$

An important feature of this representation is that it exhibits the fact that trident conversion depends principally on the parameter

$$\Upsilon=(E/mc^2)(H/H_{cr}),$$

where E, as noted above, is the energy of the initial electron.

The exact analytical form of $\hat{\Omega}(\Upsilon)$ is too cumbersome to provide any useful insight. As shown in Appendix 3, it has the asymptotic limits

$$\hat{\Omega}(\Upsilon)=\begin{cases}(\pi^{5/2}/16)(3\Upsilon)^{1/4}\exp\{-8(3\Upsilon)^{-1/2}\}, & \Upsilon\ll 1;\\ (\pi^2/2)\ln\Upsilon, & \Upsilon\gg 1.\end{cases} \quad (4.4b)$$

Numerical values may be obtained from the graph given in Fig. 12. We see that the high-energy limit—or more precisely, the large Υ limit—of $\hat{\Omega}(\Upsilon)$ does in fact exhibit the expected logarithmic behavior. The other asymptotic limit has a slightly more complicated functional dependence. This is consistent with the general trend that one would anticipate for conversion processes of increasingly higher order. Comparing with the corresponding limit of ordinary pair production, e.g. (3.3a–c), we see that trident conversion is diminished by a factor of α (second-order process!) but decreases far less rapidly with energy, i.e., exp $(-\Upsilon^{-1/2})$ as compared with exp $(-\Upsilon^{-1})$. A detailed discussion of (4.4) and an evaluation of its significance relative to other trident production processes is given in Sec. 4C.

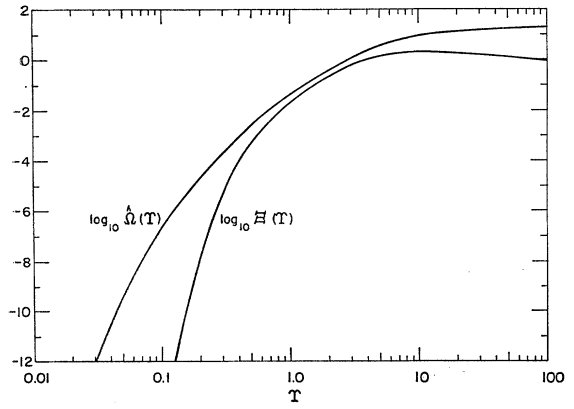

FIG. 12. Graphs of the trident production functions: $\hat{\Omega}(\Upsilon)$ and $\Xi(\Upsilon)$ correspond to virtual and real intermediate photon states, respectively. Compare Eqs. (4.4a) and (4.6b).

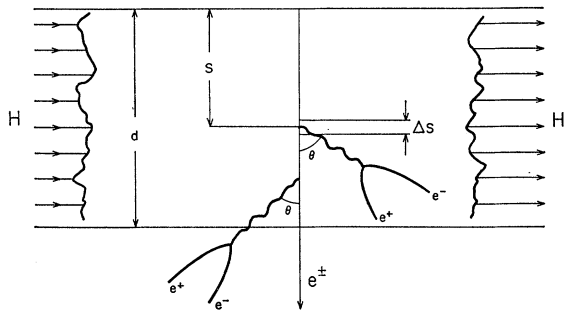

FIG. 13. Trident cascades resulting from magnetic bremsstrahlung and subsequent pair conversion. Essentially the same diagram describes the analogous processes occurring in material media. In the ultrarelativistic limit $\theta\sim\mathcal{O}(mc^2/E)\to 0$.

B. Trident Production by Real Photons

The conversion rate governing this process can be estimated by considering the two-step sequence "magnetic bremsstrahlung→magnetic pair production" which is schematically indicated on Fig. 13. The number of bremsstrahlung photons radiated into the energy interval $\Delta(h\nu)$ over a distance ΔS is given by

$$nI(E,H,h\nu)(\Delta S/c)[\Delta(h\nu)/h\nu];$$

where $nI(E,H,h\nu)$ is the spectral function corresponding to bremsstrahlung emission by n electrons with energy E traversing a perpendicular magnetic field H [compare (2.5a)]. These photons partially convert into pairs, and according to Fig. 13 and the photon attenuation equation (3.1), at a depth d one expects

$$n\alpha(\nu)I(E,H,h\nu)(d-S)(\Delta S/c)[\Delta(h\nu)/h\nu]$$

pairs to have been produced. The total number of tridents arising from real photon conversion then is given by

$$N_R^{(\Upsilon)}(E,H)=n\sum_\nu\sum_s \alpha(\nu)I(E,H,h\nu)(d-S)\times(\Delta S/c)[\Delta(h\nu)/h\nu]. \quad (4.4c)$$

This representation is analogous to Eq. (4.2) which determines the rate for virtual photon trident production. The detailed numerical evaluation of this expression of course requires explicit forms for the photon attenuation coefficient and the bremsstrahlung spectral function. It is convenient to introduce the auxiliary variables

$$\sigma=(h\nu/mc^2)(H/H_{cr}), \quad \text{and} \quad \Upsilon=(E/mc^2)(H/H_{cr}). \quad (4.5)$$

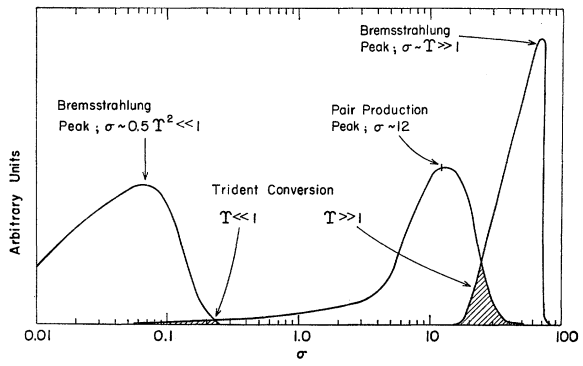

FIG. 14. Sketch of the bremsstrahlung and pair production curves for real photon trident cascades. The principal contributions to $N_R^{(T)}(E, H)$ [compare (4.4c)] arise from the cross-hatched overlap regions.

Energy conservation implies the constraint $\sigma \leq \Upsilon$. In terms of these variables we then have [compare (3.3a)]

$$\alpha(\nu) = 0.16(\alpha/\lambda\!\!\!^{-}_c)\,(H/H_{cr})\,\sigma^{-1}\,K^2_{1/3}(4/3\sigma), \quad (4.5a)$$

and [compare (2.5a)]

$$c^{-1}\,I(E, H, h\nu) = \frac{1}{3\pi^2}\,\frac{\alpha}{\lambda\!\!\!^{-}_c}\left(\frac{\sigma}{\Upsilon^2}\right)^2 \frac{H}{H_{cr}}\,\mathfrak{M}(\sigma, \Upsilon), \quad (4.5b)$$

where $\mathfrak{M}(\sigma, \Upsilon) = \mathfrak{M}(y, \Upsilon)$, represents the auxiliary function defined in Eq. (2.5b). Inserting these expressions into (4.4c), and carrying out the spatial integration, we obtain

$$N_R^{(T)}(E, H) = \frac{\sqrt{3}}{25\pi}\,n\left(\alpha\,\frac{d}{\lambda\!\!\!^{-}_c}\,\frac{H}{H_{cr}}\right)^2 \Xi(\Upsilon), \quad (4.6a)$$

where

$$\Xi(\Upsilon) = \frac{2\sqrt{3}}{9\pi}\,\Upsilon^{-4}\int_0^\Upsilon d\sigma\,\mathfrak{M}(\sigma, \Upsilon)\,K^2_{1/3}(4/3\sigma). \quad (4.6b)$$

This representation shows clearly that real photon trident cascades tend to increase quadratically with distance and field strength—as would be expected for a second-order process. The importance of the parameter Υ is also once again exhibited.

The general behavior of $\Xi(\Upsilon)$ may be inferred from the curves sketched in Fig. 14. For values of Υ less than unity, the bremsstrahlung spectrum will consist principally of low-energy photons and the probability for pair conversion will be negligibly small. In fact in the limit $\Upsilon \ll 1$ one would expect that real photon trident conversion would decrease even more rapidly than pair production. In the opposite limit ($\Upsilon \gg 1$) one would also anticipate a decrease in the conversion rate. This is essentially due to the fact that in this case most of the bremsstrahlung emission is concentrated near the high-energy end of the spectrum. Since pair production decreases in the range $\sigma < 12$, it is evident that the overlap between bremsstrahlung and photon attenuation will progressively diminish as Υ increases in magnitude. An immediate consequence of these considerations is that trident cascades mediated by virtual photons will tend to dominate in both of the ranges $\Upsilon \ll 1$ and $\Upsilon \gg 1$.

The situation sketched in Fig. 14 also suggests some analytical simplifications for expediting the evaluation of $\Xi(\Upsilon)$. First we remark that in cases where $\Upsilon \gg 1$, it is evident that only values of $\mathfrak{M}(\sigma, \Upsilon)$, corresponding to the range $\sigma \ll \Upsilon$, will contribute significantly to trident conversion. Under these circumstances we have the approximate reduction

$$\mathfrak{M}(\sigma, \Upsilon) \simeq (9\pi/2\sqrt{3})\,(\Upsilon^2/\sigma)^2\,\kappa(2\sigma/3\Upsilon^2), \quad (4.7)$$

which was derived and discussed in Sec. 2A. A particularly useful feature of this representation is that it continues to be valid in the range $\Upsilon \ll 1$, *without* the necessity for any special restrictions[16] on the values of σ. This implies that in both of the extreme cases $\Upsilon \gtrless 1$, the value of $\Xi(\Upsilon)$ may be estimated from the representation

$$\Xi(\Upsilon) \simeq \int_0^\Upsilon d\sigma\,\sigma^{-2}\,\kappa(2\sigma/3\Upsilon^2)\,K^2_{1/3}(4/3\sigma), \quad (4.8)$$

where $\kappa(z)$ is the bremsstrahlung function previously defined in equation (2.9). In Appendix 4 it is shown that in the appropriate ranges $\Xi(\Upsilon)$ is given by

$$\Xi(\Upsilon) \simeq \begin{cases} 0.4\Upsilon^{1/2}\exp(-10/3\Upsilon), & \Upsilon \ll 1; \\ 4.4\Upsilon^{-2/3}\ln\Upsilon, & \Upsilon \gg 1. \end{cases} \quad (4.9)$$

For intermediate values of $\Upsilon(\sim 1)$, Ξ must be calculated directly from (4.6b) by numerical integration. A graph of $\Xi(\Upsilon)$ is given in Fig. 12.

C. Comparison of Trident Cascades in Magnetic Fields and Material Media

It is convenient to begin these comparisons by determining which of the processes discussed in the previous sections—real or virtual photon trident production—dominates under suitable conditions. This information can easily be obtained by considering the ratio

$$[N_R^{(T)}(E, H)/N_V^{(T)}(E, H)] = 0.2[d\,H\,\Xi(\Upsilon)/\lambda\!\!\!^{-}_c\,H_{cr}\,\hat{\Omega}(\Upsilon)], \quad (4.10)$$

[16] The immediate vicinity of the bremsstrahlung tip ($\sigma \sim \Upsilon$) is excluded. In cases where $\Upsilon \ll 1$, the omission of this region is of negligible significance.

for various values of the parameters. The numerical work can be simplified by measuring distances in millimeters and magnetic field strength in units of 10 MG, i.e., $H \equiv \mathsf{H} \times 10^7$. If we also introduce logarithms (base 10), then the ratio (4.10) can be rewritten in the form

$$\log [N_R^{(T)}(E, H)/N_V^{(T)}(E, H)] = 2.1 + \log (d\mathsf{H}) + \log \Xi(\Upsilon) - \log \hat{\Omega}(\Upsilon). \quad (4.10a)$$

With the aid of the curves given in Fig. 12 it is then a straightforward matter to determine the conditions under which one or the other process is dominant.

Generally speaking, for values of $\Upsilon < 0.2$, the virtual photon trident rate tends to be greater. From an experimental point of view however this is of almost no significance since one can easily check that in this region the total trident production rate is vanishingly small. Conditions are much more favorable in the range $\Upsilon > 0.2$. Assuming that the fields and distances satisfy the requirement $d\mathsf{H} > 1$, one may verify from (4.10a) that the real photon (cascade) process dominates in this region. The magnetic trident production rate increases to the point where it can compete favorably with the corresponding process in material media. Under still more extreme conditions, i.e., values of $\Upsilon \gg 100$—which are of course experimentally very implausible—the virtual photon trident process again tends to dominate. However this is not to be taken seriously even as a theoretical indication, since damping corrections [H1] begin to alter the ratio (4.10a) for much smaller values of Υ, i.e., $1 \lesssim \Upsilon \lesssim 10$.

Trident conversion with either real or virtual photon intermediate states can of course also occur in material media. It is in fact an important component of high-energy cosmic-ray showers and has been studied with a variety of experimental techniques [A4, C3, K8]. In order to obtain estimates of these conversion rates let us again consider the passage of n electrons of energy E through a path length d in a medium which in the present instance will be supposed to be a material characterized by atomic number Z, atomic weight A, and density ρ. Just as in the corresponding magnetic case it is convenient to begin by computing the rate of trident conversions due to virtual intermediate photons. In the ultra-relativistic limit the expected number of such tridents, $\bar{N}_V^{(T)}(E, Z)$, can easily be estimated with the help of the FWW method [M5]. In analogy with (4.2) we then have

$$\bar{N}_V^{(T)}(E, Z) = n\, d\, \beta(Z) \mathfrak{N}(E, \eta\, mc^2), \quad (4.11)$$

where $\beta(Z)$ is the energy-independent photon attenuation coefficient given in (3.7), and $\mathfrak{N}(E, \eta\, mc^2)$ represents the total number of virtual photons with energies $E \geq h\nu \geq \eta\, mc^2$, present in the Fourier resolution of the field associated with an electron of energy E. Since only the high-energy limit of (4.11) is required, we have $E/mc^2 \gg \eta \gg 1$, which implicitly defines the parameter η.

Now it follows from (4.3a, b) that

$$\int^{\zeta} dx\, x^{-1} W(x) = \tfrac{1}{2}(\zeta^2 - 1) K_0^2(\zeta) + \frac{\zeta}{2}[K_0(\zeta) - \zeta K_1(\zeta)] K_1(\zeta); \quad (4.12)$$

and therefore

$$\mathfrak{N}(E, \eta\, mc^2) = \frac{2\alpha}{\pi} \int_{\eta(mc^2/E)}^{1} dx\, x^{-1} W(x); \quad (4.12a)$$

$$\simeq (\alpha/\pi) \ln^2 (E/mc^2), \qquad \text{for } E/mc^2 \gg \eta \gg 1. \quad (4.12b)$$

This finally leads to the estimate [B6]

$$\bar{N}_V^{(T)}(E, Z) = nd(\alpha^2/\pi) N_0 \lambda\!\!\!^{-}_c{}^2\, h(Z) \ln^2 (E/mc^2), \quad (4.13)$$

where $\hat{h}(Z)$ is the function defined in (3.7a), and N_0 and $\lambda\!\!\!^{-}_c$ as usual denote Avogadro's number and the Compton wavelength.

Real photon trident cascades in material media may be visualized as shown in the sketch in Fig. 13. In the ultra-relativistic limit all the reaction products essentially go in the forward direction, and so the corresponding conversion rate, which we shall denote by $\bar{N}_R^{(T)}(E, Z)$, can be written down in direct analogy with (4.4c), i.e.,

$$\bar{N}_R^{(T)}(E, Z) = n\beta(Z) \sum_{\nu} \sum_{s} I(h\nu, Z)(d - S)\, \Delta S[\Delta(h\nu)/h\nu]; \quad (4.14)$$

where the photon attenuation coefficient, $\beta(Z)$, is now given by (3.7), and $I(h\nu, Z)$ represents the rate of bremsstrahlung in material media (2.31a). The integrations in the present instance are trivial, and we find the explicit form [B7]

$$\bar{N}_R^{(T)}(E, Z) = [(7 \times 2^3)/3^5]\, n\, [d\alpha N_0 \lambda\!\!\!^{-}_c{}^2]^2\, h(Z) \hat{h}(Z) \ln (E/mc^2), \quad (4.15)$$

where $h(Z)$ and $\hat{h}(Z)$ are given by (2.31b) and (3.7a), respectively. As expected, the cascade rate increases quadratically with the distance.

The relative importance of real and virtual photon trident production in material media may now be

gauged by considering the ratio

$$\frac{\bar{N}_V^{(T)}(E,Z)}{\bar{N}_R^{(T)}(E,Z)}=2.1\times10^7\frac{\lambda\!\!\!^{-}_c}{d}\frac{\ln(E/mc^2)}{h(Z)}. \quad (4.16)$$

In the present discussion the ranges of interest for the parameters are $d\sim1$ mm, and $E/mc^2\gg1$. It is then a simple matter to verify that for $Z\lesssim13$,

$$\bar{N}_V^{(T)}(E,Z)>\bar{N}_R^{(T)}(E,Z); \quad (4.16a)$$

so that in these cases the virtual photon processes dominate.

On the other hand if we consider $Z\gtrsim29$, but restrict $E\lesssim10^3$ BeV, then

$$\bar{N}_V^{(T)}(E,Z)<\bar{N}_R^{(T)}(E,Z); \quad (4.16b)$$

so that in this range the real photon cascades dominate. In principle the two types of trident conversion can of course also be distinguished through measurements of the energy and angular distributions of the emergent particles, but this requires more refined experimental techniques and involves problems beyond the scope of the present discussion.

It is now possible to proceed with the intercomparisons of trident production rates in magnetic fields and material media. Let us consider first the ratio

$$\frac{N_R^{(T)}(E,H)}{\bar{N}_V^{(T)}(E,Z)}=3.8\times10^6\frac{d}{\lambda\!\!\!^{-}_c}\left(\frac{H}{H_{cr}}\right)^2\frac{\Xi(\Upsilon)}{\hat{h}(Z)\ln^2(E/mc^2)}; \quad (4.17)$$

which is appropriate for gauging the relative rates in the range $Z\lesssim13$. For computational purposes it is again convenient to take the logarithm of the ratio (4.17), and to measure distances in millimeters, and field intensity in units of 10 MG, i.e., $H=\mathrm{H}\times10^7$. Then since

$$0.7\lesssim\log\log(E/mc^2)\lesssim0.8 \quad \text{for } 50\text{ BeV}\lesssim E\lesssim1000\text{ BeV},$$

the energy dependence in the iterated logarithm may be ignored, and the break-even condition, $N_R^{(T)}(E,H)\sim\bar{N}_V^{(T)}(E,Z)$, expressed in the form

$$\log d\mathrm{H}^2+\log\Xi(\Upsilon)=\log\hat{h}(Z)-0.6. \quad (4.17a)$$

This is an implicit equation connecting E, H, Z, and d, which with the help of the curve given in Fig. 12, may easily be solved for various values of the parameters. In particular the beryllium ($Z=4$) and high explosives ($Z\simeq8$) break-even curves shown in Fig. 15 correspond to solutions of (4.17a) with the special choice $d=2$ mm. Comparing with the pair-production break-even curves given in Fig. 10, we see that the conditions for competitive conversion generally tend to require slightly higher energies and field strengths. The sensitivity with respect to variations of Υ, already noted in connection with other magnetic conversion processes, is again exhibited in the trident production rates. If for example we refer to Fig. 15 and consider the Be and HE break-even curves corresponding to $H\sim60$ MG, then an upward shift in energy of approximately 10%, i.e., 140 BeV to 155 BeV, changes the conversion rates from about 4×10^{-3} to 8×10^{-3}, or roughly a factor of two!

In circumstance where it is of interest to compare the relative rates of trident conversion in magnetic fields and material media with $Z\gtrsim29$, the appropriate ratio to consider is

$$\frac{N_R^{(T)}(E,H)}{\bar{N}_R^{(T)}(E,Z)}=0.8\times10^{14}\left(\frac{H}{H_{cr}}\right)^2\frac{\Xi(\Upsilon)}{h(Z)\hat{h}(Z)\ln(E/mc^2)}. \quad (4.18)$$

Since both processes involve only real intermediate photons, the distance, d, cancels in the ratio. Proceeding as before, one may readily derive an explicit equation for the break-even condition, viz.,

$$2\log\mathrm{H}+\log\Xi(\Upsilon)=\log\{h(Z)\hat{h}(Z)\}+0.5. \quad (4.18a)$$

The copper ($Z=29$) and lead ($Z=82$) curves given in Fig. 15 have been constructed from this equation. The position of these curves relative to the "complete conversion" line indicated in this figure again emphasizes the fact that extremely intense magnetic fields are excellent energy degraders for ultrahigh-energy electromagnetic showers.[17]

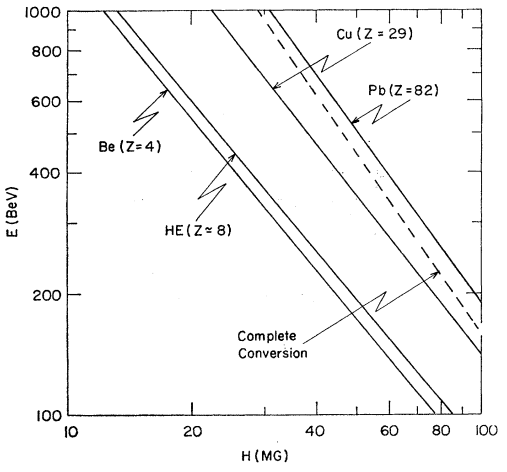

FIG. 15. Break-even conditions for trident production in magnetic fields and material media. The $Z=4$ and 8 curves correspond to (4.17a) with $d\sim2$ mm. The $Z=29$ and 82 curves are derived from (4.18a). The "complete conversion" line corresponds to $N_R^{(T)}(E,H)\sim n$, with $d\sim2$ mm.

[17] When more refined versions of these calculations are warranted, allowance will have to be made for multiple scattering corrections of the type discussed in Sec. 2D.

5. ČERENKOV RADIATION AND PHOTON SPLITTING

A. Vacuum Polarization Čerenkov Radiation

A particularly interesting aspect of quantum electrodynamic processes occurring in extremely intense electromagnetic fields is the existence of a special class of radiative modifications which are due to coherent vacuum polarization effects. Qualitatively speaking, it is not too difficult to see how such collective radiative effects could arise: The essential point is that in an approximation where vacuum polarization corrections can be described in terms of a Lagrangian of the Born–Infeld type [H2, E9], the corresponding equations governing the behavior of the electromagnetic fields include a number of nonlinear terms. These are not only responsible for light–light and light–field [Delbrück] scattering, but also permit complex propagating modes which are inherently suppressed in the linear theory. A typical example of this kind of nonlinear disturbance is the formation of electromagnetic "shock" waves; a phenomenon which has already been discussed in detail by Lutzky and Toll [L4]. If one now considers the added complication of a charged particle propagating through such vacuum polarization "plasmas," it is clear that a variety of still more complex interactions can be expected to occur. All effects of this type which are inherently nonlinear in the sense that they *cannot* be described in terms of simple perturbations of the linear theory represent collective modifications of the vacuum polarization.[18]

Under conditions where vacuum polarization may be described by a phenomenological quantum electrodynamics [J1], it can be shown that collective radiative effects will give rise to Čerenkov emission by high-energy charged particles in intense external fields. In the present section we briefly review some of the pertinent results and supplement our earlier discussions [E2, E3] with detailed comparisons of magnetic bremsstrahlung and vacuum polarization Čerenkov radiation.

Let us consider first the propagation of light through a strong external magnetic field in a direction normal to the lines of flux. Under these circumstances there will be photon–field interactions of the type shown in Fig. 8(b), and the phase velocity of light is reduced below its free space value [T1, S7]. This situation may be conveniently described by assigning an index of refraction $n(\nu)$ to the magnetic field. Quantitatively this may be derived from the forward coherent part of the scattering amplitude associated with the diagram of Fig. 8(b). This in turn may be computed from the pair-production interaction, Fig. 1(a), by means of a dispersion relation. Specifically, for the index of refraction we write

$$n(\nu)=1+\Delta n(\nu). \tag{5.1}$$

Then $\Delta n(\nu)$ can be directly obtained from the dispersion integral

$$\Delta n(\nu)=\frac{c}{2\pi^2}\int_0^\infty d\tilde{\nu}\,\frac{\alpha(\tilde{\nu})}{\tilde{\nu}^2-\nu^2}, \tag{5.2}$$

where $\alpha(\tilde{\nu})$ represents the magnetic pair-production function given in (3.3a). The explicit form of $\Delta n(\nu)$ is

$$\Delta n(\nu)=(\alpha/4\pi)\,(H/H_{\rm cr})^2\,\mathcal{G}(\chi), \tag{5.3a}$$

where

$$\mathcal{G}(\chi)=-0.027\pi^2\chi^{-2}\{K_{1/3}(\tilde{\chi})[I_{1/3}(\tilde{\chi})+I_{-1/3}(\tilde{\chi})] +2[I_{-1/3}(\tilde{\chi})\tilde{I}_{1/3}(\tilde{\chi})+I_{1/3}(\tilde{\chi})\tilde{I}_{-1/3}(\tilde{\chi})]\} \tag{5.3b}$$

and $\tilde{\chi}=\frac{2}{3}\chi=\frac{1}{3}(h\nu/mc^2)\,(H/H_{\rm cr})$ [compare (3.1)]. The "tilde" functions are derivatives of modified Bessel functions with respect to the index, i.e., $\tilde{I}_\nu\equiv(\partial/\partial\nu)I_\nu$ [E10].

The asymptotic limits of $\mathcal{G}(\chi)$ are

$$\mathcal{G}(\chi)=\begin{cases}0.22+0.30\chi^2, & \chi\ll 1;\\ -0.56\chi^{-4/3}, & \chi\gg 1.\end{cases} \tag{5.4}$$

Some numerical values of $\mathcal{G}(\chi)$ are listed in Table IX. A graph of this function is given in Fig. 16.

TABLE IX. Numerical values of $\mathcal{G}(\chi)$.

χ	$\mathcal{G}(\chi)$
0	0.22
0.17	0.23
0.22	0.24
0.40	0.25
1.00	0.17
2.22	0.059
3.33	0.027
6.66	+0.003
9.52	−0.0009

We now consider an electron with energy E traversing a magnetic field H in a direction normal to the lines of flux. At sufficiently high energies its velocity matches—and eventually exceeds—the ambient phase velocity of light. The corresponding Čerenkov threshold is then given by

$$E/mc^2\geq[2\Delta n(\nu_m)]^{-1/2}, \tag{5.5}$$

where ν_m, the frequency which *first* appears in the Čerenkov spectrum, is determined by $\mathrm{Max}\{\Delta n(\nu)\}$. In the present instance we have $\mathrm{Max}\{\mathcal{G}(\chi)\}\simeq 0.25$ for

[18] Nonperturbative binding corrections for the particle propagators are also assumed.

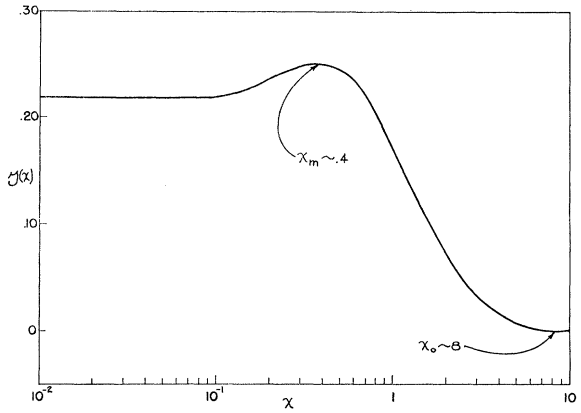

FIG. 16. Index of refraction of a magnetic field:

$$n=1+(\alpha/4\pi)\,(H/H_{cr})^2\mathcal{J}(\chi), \qquad \chi=\tfrac{1}{2}(h\nu/mc^2)\,(H/H_{cr}).$$

$\mathcal{J}(\chi)$ has a maximum at $\chi\simeq 0.4$, and crosses the abscissa at $\chi\simeq 8$.

$\chi\equiv\chi_m\simeq 0.4$; and therefore the threshold energy $E_m(\nu_m)$, associated with ν_m, is given by

$$\frac{E_m(\nu_m)}{mc^2}\,\frac{H}{H_{cr}}=\left[\frac{2\pi}{\alpha\mathcal{J}(\chi_m)}\right]^{1/2}\cong 58.5; \tag{5.6a}$$

furthermore (see Fig. 16)

$$(h\nu_m/mc^2)\,(H/H_{cr})\cong 0.8. \tag{5.6b}$$

At energies exceeding the threshold value additional frequencies will appear in the Čerenkov spectrum. Corresponding to each frequency there is a unique minimum energy $E_m(\nu)$ which marks its first appearance in the spectrum. We now introduce the notation $q(\nu)=E/E_m(\nu)$. The spectral intensity of the Čerenkov radiation then may be written in the form

$$\hat{I}(E, h\nu, H)=(2/\pi)\alpha^2(mc^2/\lambda\!\!\!^{-}_c)\chi\mathcal{J}(\chi)[1-q^{-2}(\nu)]. \tag{5.7}$$

Since Max $\{\chi\mathcal{J}(\chi)\}\simeq 0.18$ for $\chi\simeq 1.4$, one may easily check that the Čerenkov radiation rates are of the order of 12 BeV/mm. These rates are however considerably smaller than the corresponding magnetic bremsstrahlung losses. A detailed comparison can be conveniently made if we recall that the preceding relations imply the estimate

$$\frac{h\nu}{E}=\frac{2\chi}{q(\nu)}\left[\frac{2\pi}{\alpha\mathcal{J}(\chi)}\right]^{-1/2}\ll 1. \tag{5.8}$$

In this case the magnetic bremsstrahlung intensity $I(E, h\nu, H)$ is accurately represented by the expression (2.14); and the ratio of the intensities may be reduced to the compact form

$$\hat{I}(E, h\nu, H)/I(E, h\nu, H)=[0.86\alpha\chi\mathcal{J}(\chi)q(\nu)]^{2/3}[1-q^{-2}(\nu)]. \tag{5.9}$$

Just above the threshold, i.e., $q(\nu)\gtrsim 1$, this gives $\hat{I}\sim 10^{-2}I$; and therefore Čerenkov emission is negligible in these cases. There is however a strong analogy to the relation between ordinary bremsstrahlung and Čerenkov radiation in material media: The essential feature of this situation—which of course underlies the operation of all conventional Čerenkov counters—is that the low end of the observed spectrum is completely dominated by Čerenkov emission under circumstances where the radiating particle has an energy far above threshold. An analogous relation for the magnetic processes is implied by (5.9). Far above threshold we have

$$\hat{I}(E, h\nu, H)/I(E, h\nu, H)\sim 10^{-2}\,q^{2/3}(\nu), \tag{5.9a}$$

and at super-high energies Čerenkov radiation becomes dominant.[19]

In this connection it should be noted that there is an option in the spatial discrimination of bremsstrahlung and Čerenkov emission. The opening angle of the vacuum polarization Čerenkov cone is given by [E3]

$$\theta_C=(H/H_{cr})[(\alpha/2\pi)\mathcal{J}(\chi)\{1-q^{-2}(\nu)\}]^{1/2}. \tag{5.10}$$

The preferred angle for bremsstrahlung emission is $\theta_B\sim mc^2/E$; and the differential cross section in first approximation is proportional to $\sim\{1+[(E/mc^2)\theta]^2\}^{-2}$. It is then easy to show that $\theta_C\sim q(\nu)\theta_B\geq\theta_B$; and if we compare the respective radiation rates at the *larger* angle, i.e., θ_C, the ratio (5.9a) is replaced by the more conservative estimate

$$[\hat{I}(E, h\nu, H)/I(E, h\nu, H)]\,|_{\theta_C}\sim 10^{-2}\,q^{8/3}(\nu). \tag{5.11}$$

B. Photon Splitting

To lowest order photon splitting is described by the diagram shown in Fig. 2. The external fields responsible for the binding of the intermediate state pairs may of course be either electric or magnetic. At low energies, i.e., for $h\nu\ll mc^2$, and in the weak-field limit,

$$H\ll m^2c^3/e\hbar\gg\mathcal{E},$$

photon splitting can be reliably estimated from the equivalent vacuum polarization Lagrangian of the Born–Infeld theory [H2, S8]. At higher energies it is advisable to derive the results directly from quantum

[19] In particular, for $E\sim 10^{19}$ eV, $H\sim 0.1$ MG, Čerenkov radiation will dominate in the spectral region $h\nu\gtrsim 10^{14}$ eV. These estimates are of course contingent on the semiquantitative reliability of (2.14) even under conditions of strong radiative corrections.

electrodynamics. However even for the single loop diagram (Fig. 2) this calculation is extremely tedious, and the best results available correspond to Born expansions in the binding of the intermediate states. Photon splitting due to vacuum polarization has not yet been observed experimentally.

Suppose we consider a photon propagating through a uniform magnetic field in a direction normal to the lines of flux. Then according to Skobov [S9] the attenuation coefficient for photon splitting $\mathcal{S}(h\nu, H)$ is given by the expression

$$\mathcal{S}(h\nu, H)=\frac{5}{3(144\pi)^2}\frac{\alpha^3}{\lambda\!\!\!^{-}_c}\frac{h\nu}{mc^2}\left(\frac{H}{H_{cr}}\right)^2; \qquad (5.12)$$

where the principal approximation in the derivation is $H\ll H_{cr}$. It is characteristic for external field photon transformations of this type that the conversion rates are smoothly varying functions of the field strengths and photon energies. This is in sharp contrast to processes such as pair conversion where the attenuation rates diminish very rapidly for conditions such that $(h\nu/mc^2)(H/H_{cr})\gtrsim\frac{1}{3}$ [compare (3.3a–c)]. In principle therefore photon splitting may be observable under circumstances where the characteristic energies are low but very intense illumination is available. Unfortunately most schemes involving lasers or pulsed x-ray devices lead to marginal photon splitting rates and depend on optimistic estimates of the tolerable signal-to-noise ratios. If one considers high fields set up in the vicinity of material media—for example pulse-implosion generators of megagauss fields—then photon splitting at low energies ($h\nu\lesssim mc^2$) will tend to be masked by double Compton scattering in the surrounding explosives and liners.

These difficulties persist at higher energies. The principal competing processes in material media then are photon splitting in the nuclear Coulomb fields and double Compton scattering. In particular the photon splitting coefficient, analogous to (5.12), for a medium of density ρ, atomic number Z and weight A, is approximately given by [T4, B7, S6]

$$\mathcal{S}(h\nu, Z)\simeq 3.5\times10^{-8}\,\alpha^3(\alpha Z)^2\,(\rho/A)\ln(h\nu/mc^2), \qquad (5.13)$$

where it is assumed that $h\nu\gg mc^2$, and shielding corrections have been ignored. Under these conditions double Compton scattering becomes less important since the cross section is bounded from above by $\alpha^3\lambda\!\!\!^{-}_c{}^2(mc^2/h\nu)\ln(h\nu/mc^2)$. It is in fact easy to check that for energies satisfying the inequality

$$\alpha(\alpha Z)h\nu/mc^2>1, \qquad (5.14)$$

Coulomb field photon splitting will be the dominant process.

Comparing (5.12) and (5.13) it is then evident that in principle at least there are circumstances where magnetic photon splitting can compete favorably with photon splitting in material media. The order of magnitude of the break-even point is given by

$$\left(\frac{H}{H_{cr}}\right)^2\sim 4\times10^{-3}(\alpha Z)^2\frac{\rho}{A}\frac{mc^2}{h\nu}\ln\left(\frac{h\nu}{mc^2}\right); \qquad (5.15)$$

but this requires rather exotic conditions. For example, if we consider incident photon energies of the order of 300 BeV, and high explosives, i.e., $Z\simeq 8$, then magnetic photon splitting will predominate for fields in the range $\gtrsim 2\times10^8$ G. Experimentally however this is of no significance since in this case the principal photon conversion process would actually be magnetic pair production. Under more realistic circumstances, e.g., $(h\nu/mc^2)(H/H_{cr})\sim10^{-2}$, photon splitting should indeed be observable but this depends on the development of techniques for maintaining intense fields—either $H\sim10^7$ G or $\mathcal{E}\sim10^9$ V/cm—momentarily in evacuated regions.

ACKNOWLEDGMENTS

Part of this work was carried out at the Université Libre de Bruxelles. It is a pleasure to thank Professor I. Prigogine for his kind hospitality. Numerous auxiliary calculations for this paper were carried out by Dr. S. M. Prastein, H. C. Shih, and J. Schweigert. The support of the U. S. Army Research Office, Durham, is gratefully acknowledged.

APPENDIX I: INTEGRAL IDENTITIES FOR MODIFIED BESSEL FUNCTIONS

We wish to establish the modified Bessel function identity [K5]

$$y\int_y^\infty dx\,K_{5/3}(x)=\frac{\sqrt{3}}{\pi}y^2\int_0^\infty dx\{\cosh^5 x\,K^2_{2/3}(\tfrac{1}{2}y\cosh^3 x)$$
$$+\cosh^3 x\sinh^2 x\,K^2_{1/3}(\tfrac{1}{2}y\cosh^3 x)\}, \qquad y>0, \quad (A1)$$

which is substantially equivalent to that required for the transition from Eq. (2.8d) to Eq. (2.8f) of the text. The proof given here is based on a slight extension of several ideas originally due to Lerch and Hardy (p. 382 of [W1], [L2]).

Let us suppose that we are faced with the problem of verifying the equality of two functions, $f_1(y)$ and $f_2(y)$, which are specified in terms of representations (these may be integral representations) that are sufficiently complicated so that a direct comparison is rendered impractical. This problem can often be dealt with by introducing a parametric transformation of the functions to a more tractable form. Specifically, let us consider a mapping operation $\mathcal{O}(p\mid y)$ which transforms the f's according to the rule

$$\mathcal{O}(p\mid y)\,f(y)\to\hat{f}(p). \qquad (A2)$$

With an appropriate choice of $\mathcal{O}(p \mid y)$ it may then be possible to simplify the explicit form of the $\hat{f}$'s to the point where the identity $\hat{f}_1=\hat{f}_2$ can in fact be established directly. Schematically this entire process may be represented by the diagram:

$$\begin{array}{ccc} f_1(y) & \stackrel{?}{=} & f_2(y) \\ \Updownarrow & & \Updownarrow \\ \mathcal{O}(p \mid y)\, f_1(y) \equiv \hat{f}_1(p) = \hat{f}_2(p) & \equiv & \mathcal{O}(p \mid y)\, f_2(y). \end{array} \tag{A3}$$

The essential links in this sequence are the proof of the invertibility of the mapping (A2), and the explicit verification of the identity $\hat{f}_1=\hat{f}_2$. In the present instance a convenient choice for the operator $\mathcal{O}(p \mid y)$ is the Mellin transform, i.e.,

$$\mathcal{O}(p \mid y)\, f(y) \rightarrow \int_0^\infty dy\, y^p f(y) = \hat{f}(p); \tag{A4}$$

since this permits an elementary computation of the $\hat{f}$'s, and leads to a unified treatment of the comparison question ($\hat{f}_1=\hat{f}_2$), within the general framework of the Stieltjes' moment problem [W2].

We begin with the obvious identifications

$$f_1(y) \equiv y \int_y^\infty dx\, K_{5/3}(x), \tag{A5a}$$

and

$$f_2(y) \equiv \frac{\sqrt{3}}{\pi} y^2 \int_0^\infty dx\, \{\cosh^5 x\, K^2_{2/3}(\tfrac{1}{2} y \cosh^3 x) + \cosh^3 x \sinh^2 x\, K^2_{1/3}(\tfrac{1}{2} y \cosh^3 x)\}. \tag{A5b}$$

It is also convenient to restrict the $\hat{f}(p)$'s of (A4) to integer values of the argument so that they reduce to simple moments. For these we introduce the notation

$$C_n^{(1)} = \int_0^\infty dy\, y^n f_1(y), \qquad n=0, 1, \cdots; \tag{A6a}$$

and

$$C_n^{(2)} = \int_0^\infty dy\, y^n f_2(y), \qquad n=0, 1, \cdots. \tag{A6b}$$

At this point we invoke the *sufficient* conditions for the uniqueness of the Stieltjes' moment problem. These may be concisely stated in terms of

Carleman's Theorem [C2]: Suppose that we have two nonnegative functions

$$f_1(y) \geq 0, \quad \text{and} \quad f_2(y) \geq 0; \tag{A7a}$$

for which an infinite sequence of moments is equal,

$$C_n^{(1)} = C_n^{(2)}, \qquad n=0, 1, 2, \cdots. \tag{A7b}$$

If these moments satisfy the divergence criterion

$$\sum_n^\infty (1/C_n)^{1/2n} \rightarrow \infty; \tag{A7c}$$

then the conclusion is that the moment problem does have a unique solution, i.e.,

$$f_1(y) \equiv f_2(y). \tag{A7d}$$

Carleman's theorem therefore insures that with appropriate conditions the mapping (A2) is indeed invertible. The explicit proof of the basic identity (A1) is now reduced to checking that all the analytical details involved in the sequence (A3) are in fact consistent with the hypotheses (A7a) through (A7c).

The first condition (A7a) may easily be satisfied by requiring that $y>0$ in (A5a) and (A5b). The next step consists of verifying that all the moments are indeed equal. This requires the explicit calculation of (A6a) and (A6b). A number of auxiliary integrals are useful in this connection:

$$\int_0^\infty du (\cosh u)^{-\tau} = 2^{\tau-2}[\Gamma(\tau/2)]^2/\Gamma(\tau), \qquad \tau>0$$

$$\int_0^\infty du\, u^\sigma K_\nu(u) = 2^{\sigma-1}\, \Gamma[\tfrac{1}{2}(\sigma+1-\nu)]\Gamma[\tfrac{1}{2}(\sigma+1+\nu)], \qquad \mathrm{Re}\{\sigma+1\} > |\,\mathrm{Re}\{\nu\}\,|,$$

$$\int_0^\infty du\, u^\sigma K_\nu^2(u) = 2^{\sigma-2}\, \Gamma[\tfrac{1}{2}(\sigma+1)+\nu]\Gamma[\tfrac{1}{2}(\sigma+1)-\nu] \times (\Gamma[\tfrac{1}{2}(\sigma+1)])^2/\Gamma(\sigma+1), \qquad \mathrm{Re}\{\sigma+1\} > 2\,|\,\mathrm{Re}\{\nu\}\,|. \tag{A8}$$

Then

$$C_n^{(1)} = \int_0^\infty dy\, y^{n+1} \int_y^\infty dx\, K_{5/3}(x) = (n+2)^{-1} \int_0^\infty dy\, y^{n+2} K_{5/3}(y), \tag{A9a}$$

or

$$C_n^{(1)} = \frac{2^{n+1}}{n+2}\, \Gamma[\tfrac{1}{2}(n+3)+\tfrac{5}{6}]\Gamma[\tfrac{1}{2}(n+3)-\tfrac{5}{6}]. \tag{A9b}$$

For the other moments we make the decomposition

$$C_n^{(2)} = (\sqrt{3}/\pi)\,(\mathcal{J}_1+\mathcal{J}_2), \tag{A10a}$$

where

$$\mathcal{J}_1 = \int_0^\infty dy \int_0^\infty dx\, y^{n+2} K^2_{1/3}(\tfrac{1}{2} y \cosh^3 x)\, \cosh^3 x \sinh^2 x, \tag{A10b}$$

and

$$\mathcal{J}_2=\int_0^\infty dy\int_0^\infty dx\, y^{n+2}\,K^2_{2/3}(\tfrac{1}{2}y\cosh^3 x)\,\cosh^5 x. \tag{A10c}$$

Introducing the new variable $u=\frac{1}{2}y\cosh^3 x$ in both integrals,[20] we find

$$\mathcal{J}_1=\int_0^\infty dx\left(\frac{2}{\cosh^3 x}\right)^{n+3}\cosh^5 x\sinh^2 x \times\int_0^\infty du\,u^{n+2}\,K^2_{1/3}(u), \tag{A10d}$$

and

$$\mathcal{J}_2=\int_0^\infty dx\left(\frac{2}{\cosh^3 x}\right)^{n+3}\cosh^5 x\int_0^\infty du\,u^{n+2}\,K^2_{2/3}(u). \tag{A10e}$$

With the help of the auxiliary integrals (A8), these quadratures may be carried out explicitly,

$$\mathcal{J}_1=\frac{2^{5(n+1)}}{3n+5}\,\Gamma[\tfrac{1}{2}(n+3)+\tfrac{1}{3}]\Gamma[\tfrac{1}{2}(n+3)-\tfrac{1}{3}] \times(\Gamma[\tfrac{1}{2}(n+3)]\Gamma(\tfrac{3}{2}n+2))^2/(\Gamma(3n+4)\,\Gamma(n+3)), \tag{A10f}$$

and

$$\mathcal{J}_2=2^{5(n+1)}\,\Gamma[\tfrac{1}{2}(n+3)+\tfrac{2}{3}]\Gamma[\tfrac{1}{2}(n+3)-\tfrac{2}{3}] \times(\Gamma[\tfrac{1}{2}(n+3)]\Gamma(\tfrac{3}{2}n+2))^2/(\Gamma(3n+4)\,\Gamma(n+3)). \tag{A10g}$$

Finally, (A10a), (A10f), and (A10g) may be combined to give

$$C_n^{(2)}=\sqrt{3}\,2^n\,\frac{\Gamma(\frac{3}{2}n+2)\,\Gamma[\frac{1}{2}(n+3)]}{\Gamma(\frac{3}{2}n+2+\frac{1}{2})\,\Gamma(\frac{1}{2}n+2)} \times\{\Gamma[\tfrac{1}{2}(n+3)+\tfrac{2}{3}]\Gamma[\tfrac{1}{2}(n+3)-\tfrac{2}{3}] +(3n+5)^{-1}\,\Gamma[\tfrac{1}{2}(n+3)+\tfrac{1}{3}]\Gamma[\tfrac{1}{2}(n+3)-\tfrac{1}{3}]\}. \tag{A11}$$

Elementary computations now yield the special values:

$$C_0^{(1)}=C_0^{(2)}=(8/3^{5/2})\pi,$$
$$C_1^{(1)}=C_1^{(2)}=(5\times 11/3^4)\pi, \tag{A12}$$
$$C_2^{(1)}=C_2^{(2)}=(7\times 32/3^{9/2})\pi,$$

These provide the basis for an inductive proof of the identity of $C_n^{(1)}$ and $C_n^{(2)}$. It is convenient to carry the induction from n to $n+2$. The key step is the verification of the equality $C^{(1)}{}_{n+2}=C^{(2)}{}_{n+2}$, expressed in terms of (A9b) and (A11). This can be reduced to establishing the identity

$$[2/(n+4)]\Gamma[\tfrac{1}{2}(n+5+\tfrac{5}{3})]\Gamma[\tfrac{1}{2}(n+5-\tfrac{5}{3})] =3^{-1/2}\,\frac{\Gamma(\frac{3}{2}n+5)\Gamma[\frac{1}{2}(n+3)+1]}{\Gamma[\frac{1}{2}(3n+1)+5]\Gamma(\frac{1}{2}n+3)} \times\{\Gamma[\tfrac{1}{2}(n+3)+1+\tfrac{2}{3}]\Gamma[\tfrac{1}{2}(n+3)+1-\tfrac{2}{3}] +(3n+11)^{-1}\,\Gamma[\tfrac{1}{2}(n+3)+1+\tfrac{1}{3}] \times\Gamma[\tfrac{1}{2}(n+3)+1-\tfrac{1}{3}]\},\qquad n=0,1,\cdots. \tag{A13}$$

Elementary algebraic reductions show that this identity hinges on the validity of the equation

$$\frac{3j+5}{3j+7}=\frac{\Gamma[\frac{1}{2}(j+3)+\frac{1}{3}]\Gamma[\frac{1}{2}(j+3)-\frac{1}{3}]}{\Gamma[\frac{1}{2}(j+3)+\frac{2}{3}]\Gamma[\frac{1}{2}(j+3)-\frac{2}{3}]},\qquad j=0,1,\cdots; \tag{A14}$$

and this in turn depends on the auxiliary lemmas

$$\frac{3j+4}{3j+5}=\frac{1}{2}\prod_{m=1}^{j+1}\frac{1-(1/3m)^2}{1-(2/3m)^2},\qquad j=0,1,\cdots; \tag{A15a}$$

and

$$\frac{6j+5}{6j+7}=-\prod_{m=1}^{j+1}\frac{1-(2/[3(2m-1)])^2}{1-(4/[3(2m-1)])^2},\qquad j=0,1,\cdots. \tag{A15b}$$

It can easily be verified that this entire sequence of implications may be reversed: (A15b) and (A15a) together yield (A14); this in turn implies (A13); and in view of (A12) an appeal to induction finally establishes the equality of the moments, $C_n^{(1)}=C_n^{(2)}$. The remaining divergence criterion (A7c) now follows as an elementary consequence of Stirling's approximation applied to the C_n's. We find

$$C_n^{(1)}=C_n^{(2)}\approx\pi\,n^{n+1}\,e^{-n}\qquad\text{for } n\gg 1; \tag{A16}$$

and this implies

$$\sum_n^\infty (1/C_n)^{1/2n}\to\sum_n^\infty n^{-1/2}\to\infty. \tag{A17}$$

All the hypotheses of Carleman's theorem are thereby satisfied and in virtue of (A3) and (A7d) the equality of both sides of (A1) is proved.

[20] These interchanges can be justified on the basis of absolute convergence.

A related expression is the index-shifting representation

$$K_\nu(z)=\left(\frac{2z}{\pi}\right)^{1/2}\int_0^\infty d\tau(\cosh\tau)^{\nu+1/2}\,K_{\nu-1/2}(z\cosh\tau),$$
$$z>0,\ \mathrm{Im}\,\{\nu\}=0, \quad \text{(A18)}$$

which arises in connection with calculations of trident cascades (Sec. 4). This identity may be verified by methods similar to those of the above. Here

$$f_1(y)=K_\nu(y), \quad \text{(A19a)}$$

and

$$f_2(y)=\left(\frac{2y}{\pi}\right)^{1/2}\int_0^\infty d\tau(\cosh\tau)^{\nu+1/2}\,K_{\nu-1/2}(y\cosh\tau). \quad \text{(A19b)}$$

Then

$$C_n^{(1)}=\int_0^\infty dy\,y^n\,K_\nu(y)$$
$$=2^{n-1}\,\Gamma[\tfrac{1}{2}(n+1-\nu)]\Gamma[\tfrac{1}{2}(n+1+\nu)], \quad \text{(A20a)}$$

and

$$C_n^{(2)}=\left(\frac{2}{\pi}\right)^{1/2}\int_0^\infty dy\int_0^\infty d\tau\,y^{n+1/2}$$
$$\times(\cosh\tau)^{\nu+1/2}\,K_{\nu-1/2}(y\cosh\tau). \quad \text{(A20b)}$$

Introducing the new variable $\chi=y\cosh\tau$, and presuming sufficiently large values for the moment index[21] n, i.e., $n>\nu-2$, (A20b) may be transformed to

$$C_n^{(2)}=\left(\frac{2}{\pi}\right)^{1/2}\int_0^\infty d\tau(\cosh\tau)^{\nu-n-1}\int_0^\infty d\chi\,\chi^{n+1/2}\,K_{\nu-1/2}(\chi),$$
$$=\frac{2^{2n-\nu-1}}{\pi^{1/2}}\,\Gamma[\tfrac{1}{2}(n+1+\nu)]\Gamma[\tfrac{1}{2}(n+2-\nu)]$$
$$\times(\Gamma[\tfrac{1}{2}(n+1-\nu)])^2/\Gamma(n+1-\nu). \quad \text{(A20c)}$$

These expressions for the moments are sufficiently simple so that their equivalence can be established without recourse to an inductive proof: A few elementary cancellations show that the conditions $C_n^{(1)}=C_n^{(2)}$, in this instance, reduce to

$$\Gamma(n+1-\nu)=(2^{n-\nu}/\pi^{1/2})\,\Gamma[\tfrac{1}{2}(n+1-\nu)]\Gamma[\tfrac{1}{2}(n+2-\nu)], \quad \text{(A20d)}$$

and this of course is immediately recognizable as an identity equivalent Legendre's duplication formula.

Finally, we note the asymptotic estimates

$$C_n^{(1)}=C_n^{(2)}\approx\pi\exp[-(n+1)]n^n, \qquad n\gg1. \quad \text{(A21a)}$$

These lead to

$$\sum_n^\infty(1/C_n)^{1/2n}\to\sum_n^\infty n^{-1/2}\to\infty, \quad \text{(A21b)}$$

and evidently Carleman's divergence criterion is once more satisfied. (A21b) and (A20d) together then insure the invertibility of the mapping (A2), and this completes the proof of the validity of (A18).[22]

APPENDIX 2: PROPERTIES OF THE BREMSSTRAHLUNG FUNCTION $\kappa(z)$

The function $\kappa(z)$ is defined by the integral representation

$$\kappa(z)=z\int_z^\infty dx\,K_{5/3}(x), \quad \text{(A22)}$$

where $K_{5/3}(x)$ is a modified Bessel function. Evidently for $z\geq0$, the function $\kappa(z)$ is nonnegative. We have the special values $\kappa(0)=\kappa(\infty)=0$; and note that $\kappa(z)$ has a broad maximum in the vicinity of $z\sim3$. More precisely, Max $\{\kappa(z)\}=\kappa(.28)=0.925$, and this value of z of course also coincides with a zero of the derivative, viz.

$$\kappa'(z)=z^{-1}\,\kappa(z)-\{\tfrac{4}{3}K_{2/3}(z)+zK_{1/3}(z)\}. \quad \text{(A23)}$$

The general behavior of $\kappa(z)$ is indicated graphically in Fig. 3; numerical values are given in Table I.

Another representation for $\kappa(z)$, especially suited for computations in the range $0\leq z\leq2$, may be obtained from (A22) with the help of the Bessel function transformation

$$K_{5/3}(x)=-\{K_{1/3}(x)+2K'_{2/3}(x)\}.$$

This leads to the expression

$$\kappa(z)=z\left\{-\frac{\pi}{\sqrt{3}}+2K_{2/3}(z)+\int_0^z dx\,K_{1/3}(x)\right\}, \quad \text{(A24)}$$

in which the $z\to0$ limit is no longer troublesome in the limits of integration. We now insert the series expansion

$$K_\nu(x)=\frac{\pi/2}{\sin(\nu\pi)}\left\{(x/2)^{-\nu}\sum_{n=0}^\infty\frac{(x/2)^{2n}}{n!\Gamma(n-\nu+1)}\right.$$
$$\left.-(x/2)^\nu\sum_{n=0}^\infty\frac{(x/2)^{2n}}{n!\Gamma(n+\nu+1)}\right\}; \quad \text{(A25)}$$

[21] Strictly speaking (A7b) must hold only for an infinite set of moments $n\geq N>0$; the particular value of n corresponding to the "first" moment is actually irrelevant. The requirement $n>\nu-2$ can therefore always be met.

[22] The method of moments does not of course yield the most general conditions for the validity of (A1) and (A18). The hypotheses may be considerably relaxed by an appeal to analytic continuation in both the "argument" and "index" variables.

and carry out the integration:

$$\int_0^z dx\, K_{1/3}(x) \equiv \hat{K}(z) = 2.53143825 z^{2/3}[1+0.09375000 z^2+0.00401786 z^4+0.00008789 z^6+\mathcal{O}(z^8)]$$
$$-1.20910963 z^{4/3}[1+0.07500000 z^2+0.00251116 z^4+0.00004566 z^6+\mathcal{O}(z^8)] \quad \text{(A26)}$$

Since $K_{2/3}(z)$ is a widely tabulated function, (A26) and (A24) are a convenient means for obtaining numerical values of $\kappa(z)$ for $0 \leq z \leq 2$ to better than $\frac{1}{2}\%$ accuracy (see Table X). The leading terms for very small z are

$$\kappa(z) \cong 2.1495\, z^{1/3} - 1.8138\, z + \mathcal{O}(z)^{7/3}, \qquad z \ll 1. \quad \text{(A27)}$$

The computation of $\kappa(z)$ for values of $z \geq 4$ may be based on the exact transformation

$$\int_z^\infty dx \left[1+\frac{7}{2}\left(\frac{4}{3x}\right)^4\right] K_{5/3}(x) = \frac{2}{3z} K_{1/3}(z) \left[1+2\left(\frac{4}{3z}\right)^2\right]$$
$$+ K_{2/3}(z) \left[1-\frac{1}{2}\left(\frac{4}{3z}\right)^2+\left(\frac{4}{3z}\right)^4\right]. \quad \text{(A28)}$$

In case $z>0$, the integral may be simplified with the mean value theorem, i.e.,

$$\int_z^\infty dx \left[1+\frac{7}{2}\left(\frac{4}{3x}\right)^4\right] K_{5/3}(x)$$
$$= \left[1+\frac{7}{2}\left(\frac{4}{3x_0}\right)^4\right] \int_z^\infty dx\, K_{5/3}(x); \qquad x_0 \geq z. \quad \text{(A28a)}$$

For values of $z \gtrsim 4$, the terms of order z^{-4} may be dropped, and we find the expression

$$\kappa(z) \cong \tfrac{2}{3} K_{1/3}(z)[1+2(4/3z)^2]+z K_{2/3}(z)[1-\tfrac{1}{2}(4/3z)^2]. \quad \text{(A29)}$$

The accuracy of this approximation is better than 4% for $z \sim 4$; and better than 1% for $z \gtrsim 5.7$.

Finally, for $z \gg 1$, we have the asymptotic estimate

$$\kappa(z) \to 1.2533\, z^{1/2} e^{-z}; \quad \text{(A30)}$$

but this is not well suited for numerical work.

APPENDIX 3: EVALUATION OF THE AUXILIARY FUNCTION $\hat{\Omega}(\Upsilon)$

In connection with estimates of trident production by virtual photons it is necessary to compute the function

$$\hat{\Omega}(\Upsilon) = \int_0^\infty du\, u^{-2}\, W(u/\Upsilon) K^2_{1/3}(4/3u), \quad \text{(A31)}$$

where W represents the Weizsäcker–Williams spectral distribution given in (4.3b), and K_ν, $\nu=\frac{1}{3}$, etc., denotes a modified Bessel function. It is convenient to introduce the integral representation

$$W(x) = \int_x^\infty d\sigma\, \sigma\, K_1^2(\sigma); \quad \text{(A32)}$$

and carry through the calculations with the auxiliary variable $\beta \equiv \frac{4}{3}\Upsilon^{-1}$. The quantity to be evaluated then is

$$\hat{\Omega}(\Upsilon) \equiv \Omega(\beta) = \int_0^\infty du \int_{4u\beta/3}^\infty d\sigma\, u^{-2}\sigma K_1^2(\sigma) K^2_{1/3}(4/3u). \quad \text{(A33)}$$

This form suggests that it is advantageous to consider the derivative $\Omega'(\beta)$. Absorbing the 4/3-factor into the u-integration, we have

$$\Omega'(\beta) = -\beta \int_0^\infty du\, K_1^2(\beta u) K^2_{1/3}(u^{-1}). \quad \text{(A34)}$$

Since convergence is not a problem here, we can intro-

TABLE X. Values of the auxiliary function $\hat{K}(z)$.

z	$\hat{K}(z)$	z	$\hat{K}(z)$
0.01	0.1148	0.2	0.7271
0.02	0.1799	0.3	0.8995
0.03	0.2331	0.4	1.034
0.04	0.2795	0.5	1.143
0.05	0.3213	0.6	1.234
0.06	0.3596	0.7	1.310
0.07	0.3952	0.8	1.374
0.08	0.4285	0.9	1.429
0.09	0.4599	1.0	1.476
0.1	0.4897	2.0	1.71

duce the integral reduction

$$K_\nu^2(z)=2\int_0^\infty d\tau\, K_0(2z\cosh\tau)\cosh(2\nu\tau),$$
$$|\arg(z)|<\pi/2 \quad \text{(A34a)}$$

for both of the Bessel functions in (A34), and so obtain

$$\Omega'(\beta)=-4\beta\int_0^\infty du\int_0^\infty d\tau\int_0^\infty d\rho\cosh(2\tau)\cosh(\tfrac{2}{3}\rho)$$
$$\times K_0([2\beta\cosh\tau]u)K_0([2\cosh\rho]u^{-1}). \quad \text{(A35)}$$

Interchanging the orders of integration, and recalling the identity

$$\int_0^\infty du\, K_\nu(\alpha u)K_\nu(\beta u^{-1})=(\pi/\alpha)K_{2\nu}(2[\alpha\beta]^{1/2});$$
$$\mathrm{Re}(\alpha)>0,\ \mathrm{Re}(\beta)>0; \quad \text{(A35a)}$$

we find

$$\Omega'(\beta)=-2\pi\int_0^\infty d\tau\int_0^\infty d\rho\cosh(2\tau)\cosh(\tfrac{2}{3}\rho)$$
$$\times[\cosh\tau]^{-1}K_0(4[\beta\cosh\tau\cosh\rho]^{1/2}). \quad \text{(A36)}$$

It is convenient to reduce this further by inserting the representation

$$K_0(2[\alpha\beta]^{1/2})=\frac{1}{2}\int_0^\infty d\hat{u}\,\hat{u}^{-1}\exp\{-(\alpha\hat{u}+\beta\hat{u}^{-1})\};$$
$$\alpha>0,\ \beta>0. \quad \text{(A37)}$$

This leads to

$$\Omega'(\beta)=-\pi\int_0^\infty d\tau\int_0^\infty d\rho\int_0^\infty d\hat{u}\cosh(2\tau)\cosh(\tfrac{2}{3}\rho)$$
$$\times[\hat{u}\cosh\tau]^{-1}\exp\{-(\hat{u}\cosh\rho+4\beta\hat{u}^{-1}\cosh\tau)\}. \quad \text{(A38)}$$

Again there are no convergence problems, and we may differentiate with respect to β. The τ and ρ integrals are then expressible in terms of Bessel functions. It is also convenient to change variables $\hat{u}\to u^{-1}$; the final result of these operations is

$$\Omega''(\beta)=4\pi\int_0^\infty du\, K_2(4\beta u)K_{2/3}(u^{-1}). \quad \text{(A39)}$$

Comparing with (A34) we see that the net gain has been the elimination of the squares of the Bessel functions in the integral representation. In fact using known generalizations of the identity (A35a) for unequal indices of the Bessel functions, it is straightforward to obtain closed forms for $\Omega(\beta)$ from (A39) in terms of generalized hypergeometric functions. This is however superfluous for our present purposes, and it will be sufficient to derive asymptotic expansions from (A39).

We begin by remarking that $K_\nu(z)$ is an increasing function of ν for positive values of z and ν. This leads to the double inequality

$$\int_0^\infty du\, K_{2/3}(4\beta u)K_{2/3}(u^{-1})<\int_0^\infty du\, K_2(4\beta u)K_{2/3}(u^{-1})<\int_0^\infty du\, K_2(4\beta u)K_2(u^{-1}). \quad \text{(A40)}$$

Applying the identity (A35a), we obtain the bounds

$$K_{4/3}(4\beta^{1/2})<(\beta/\pi^2)\Omega''(\beta)<K_4(4\beta^{1/2}). \quad \text{(A41)}$$

Suppose now that $\beta\gg1$; then both sides of the inequality approach each other since the leading terms of the asymptotic expansion of the Bessel functions are independent of the index. This yields the estimate

$$\Omega''(\beta)\to2^{-3/2}(\pi^2/\beta)^{5/4}\exp\{-4\beta^{1/2}\},\qquad \beta\gg1. \quad \text{(A42)}$$

In the present instance integration of this asymptotic estimate is legitimate. Recalling $\Omega'(\infty)=\Omega(\infty)=0$, and reconverting to $\hat{\Omega}(\Upsilon)$, we find

$$\hat{\Omega}(\Upsilon)\to(\pi^{5/2}/16)(3\Upsilon)^{1/4}\exp\{-8(3\Upsilon)^{-1/2}\},\qquad \Upsilon\ll1. \quad \text{(A43)}$$

This is one of the limiting forms given in Eq. (4.4b) of the text.

The asymptotic expansion of $\Omega(\beta)$ for $\beta\to0$, can also be conveniently derived from (A39). We insert the representation

$$K_\nu(\alpha z)=\frac{(2z)^\nu\Gamma(\nu+\frac{1}{2})}{\alpha^\nu\Gamma(\frac{1}{2})}\int_0^\infty dv\,\frac{\cos(\alpha v)}{(v^2+z^2)^{\nu+1/2}},$$
$$\mathrm{Re}\{\nu+\tfrac{1}{2}\}\geq0,\ |\arg z|<\pi/2,\ \alpha>0, \quad \text{(A44)}$$

for $K_2(4\beta u)$ in (A39). The result may be written as

$$\Omega''(\beta)=\tfrac{3}{4}\pi\beta^{-2}\mathfrak{M}(\beta), \quad \text{(A45a)}$$

where

$$\mathfrak{M}(\beta)=\int_0^\infty du\int_0^\infty dv\,\frac{u^2\cos(4\beta v)}{(u^2+v^2)^{5/2}}K_{2/3}(u^{-1}). \quad \text{(A45b)}$$

It can easily be verified that $\mathfrak{M}(\beta)$ has a series expansion about the origin; and in particular that $\mathfrak{M}(0)=\frac{2}{3}\pi$.

Combining this with (A45a), and keeping only the dominant terms, we find the asymptotic estimate

$$\Omega(\beta)\rightarrow -(\pi^2/2)\ln\beta, \qquad \beta\ll 1. \tag{A46}$$

Since $\Omega(\beta)=\hat{\Omega}(\Upsilon)$, this leads to the expression corresponding to $\Upsilon\gg 1$ given in (4.4b).

APPENDIX 4: EVALUATION OF THE AUXILIARY FUNCTION $\Xi(\Upsilon)$

This function is defined in terms of the integral representation

$$\Xi(\Upsilon)=\int_0^{\Upsilon} d\sigma\,\sigma^{-2}\,\kappa\left(\frac{2\sigma}{3\Upsilon^2}\right)K^2_{1/3}\left(\frac{4}{3\sigma}\right), \tag{A47}$$

where

$$\kappa(z)=z\int_z^{\infty} dx\,K_{5/3}(x).$$

As shown in the discussion of Sec. 4B the evaluation of the rate of trident production for real photon intermediate states requires estimates of $\Xi(\Upsilon)$ corresponding to both of the ranges $\Upsilon\gg 1$ and $\Upsilon\ll 1$.

It is convenient to begin by considering the case $\Upsilon\gg 1$. The argument of the bremsstrahlung function $\kappa(z)$ in this instance is always very much less than unity and it is possible to use the simplifying approximation [compare (2.12)]

$$\kappa(z)\simeq 2.15\,z^{1/3}.$$

The basic integral representation (A47) can then be rewritten in the form

$$\Xi(\Upsilon)\simeq 1.55\,\Upsilon^{-2/3}\,\xi(\tau_0,\Upsilon), \qquad \Upsilon\gg 1; \tag{A48a}$$

where

$$\xi(\tau_0,\Upsilon)=\int_{4/3\tau_0}^{\infty} d\tau\,\tau^{-1/3}\,K^2_{1/3}(\tau). \tag{A48b}$$

Since the bremsstrahlung spectrum is not well represented by $\kappa(2\sigma/3\Upsilon^2)$ in the region of the tip, i.e., the range $\sigma\rightarrow\Upsilon$, it is advisable to cut off the integration at a lower energy. This is the significance of the auxiliary constant τ_0, where $1\ll\tau_0<\Upsilon$, which has been introduced in (A48b). In order to obtain the leading term of $\Xi(\Upsilon)$ for $\Upsilon\gg 1$, we now perform a parts integration, viz.

$$\xi(\tau_0,\Upsilon)=-\left(\frac{4}{3\tau_0}\right)^{2/3}\ln\left(\frac{4}{3\tau_0}\right)K^2_{1/3}\left(\frac{4}{3\tau_0}\right) - \int_{4/3\tau_0}^{\infty} d\tau\ln\tau\,\frac{d}{d\tau}\left[\tau^{2/3}\,K^2_{1/3}(\tau)\right]. \tag{A49a}$$

It is easy to check that this reduces to the expression

$$\xi(\tau_0,\Upsilon)\simeq\left[2^{-2/3}\,\Gamma(\tfrac{1}{3})\right]^2\ln(3\tau_0/4) + \mathcal{O}(\tau_0^{-2/3}\ln\tau_0), \qquad \text{for } \tau_0\gg 1. \tag{A49b}$$

The uncertainty regarding the contribution of the bremsstrahlung tip now enters only through the slowly varying factor $\ln\tau_0$. For our present purposes it is sufficient to single out the limit $\xi(\Upsilon,\Upsilon)$ which, in conjunction with the previous results, then leads to the compact estimate

$$\Xi(\Upsilon)\simeq 4.4\,\Upsilon^{-2/3}\ln\Upsilon, \qquad \Upsilon\gg 1. \tag{A50}$$

Similar methods can be used to obtain approximations for $\Xi(\Upsilon)$ which are valid in the range $\Upsilon\ll 1$. In this case it is possible to take advantage of the asymptotic expansion

$$K^2_{1/3}(4/3\sigma)\simeq(3\pi/8)\sigma\exp(-8/3\sigma), \qquad \sigma\ll 1;$$

to simplify the integrand of (A47). It is convenient to introduce the abbreviation $p\equiv 8/9\Upsilon^2$, and rearrange the variables of integration. $\Xi(\Upsilon)$ can then be represented in the form

$$\Xi(\Upsilon)\simeq(3\pi/8)\,p\,\xi(\Upsilon), \qquad \Upsilon\gg 1, \tag{A51a}$$

where

$$\xi(\Upsilon)=\int_0^{3\Upsilon/4} d\tau\,e^{-2/\tau}\int_{p\tau}^{\infty} dx\,K_{5/3}(x). \tag{A51b}$$

This expression can be simplified still further with the help of the identity

$$\xi(\Upsilon)+\xi_1(\Upsilon)-\tfrac{1}{2}\xi_2(\Upsilon)=\tfrac{3}{8}(\Upsilon/p)\exp(-8/3\Upsilon)\,\kappa(\tfrac{3}{4}p\Upsilon); \tag{A52a}$$

where

$$\xi_1(\Upsilon)=\int_0^{3\Upsilon/4} d\tau\,\tau\,e^{-2/\tau}\int_{p\tau}^{\infty} dx\,K_{5/3}(x), \tag{A52b}$$

and

$$\xi_2(\Upsilon)=p\int_0^{3\Upsilon/4} d\tau\,\tau^2\,e^{-2/\tau}\,K_{5/3}(p\tau). \tag{A52c}$$

Now in virtue of the mean value theorem we have

$$\xi_1(\Upsilon)=\bar{\tau}\,\xi(\Upsilon), \qquad \text{where } 0\leq\bar{\tau}\leq\tfrac{3}{4}\Upsilon. \tag{A53}$$

Since Υ itself is bounded from above by $\Upsilon\ll 1$, we may obviously neglect ξ_1 relative to ξ in Eq. (A52a).

The auxiliary function $\xi_2(\Upsilon)$ can be dealt with by analogous methods. For this purpose it is useful to note the

Lemma:

$$y(1+y)^{-1}\,K_{5/3}(y)\leq\frac{5}{3}\int_y^{\infty} dx\,K_{5/3}(x), \qquad y>0. \tag{A54}$$

This inequality may be verified by considering the function

$$Q(y)\equiv y(1+y)^{-1}K_{5/3}(y)\Big/\int_y^\infty dx\,K_{5/3}(x), \qquad y>0. \tag{A55}$$

From the mean value theorem it follows that

$$Q(y)=\left.\frac{\dfrac{d}{dy}\{y(1+y)^{-1}K_{5/3}(y)\}}{\dfrac{d}{dy}\left\{\displaystyle\int_y^\infty dx\,K_{5/3}(x)\right\}}\right|_{y=y_0},$$

$$\text{for some } y_0\geq y. \tag{A56a}$$

Carrying out the differentiations, we obtain

$$Q(y)=(1+y_0)^{-1}\{\tfrac{5}{3}-(1+y_0)^{-1}+y_0[K_{2/3}(y_0)/K_{5/3}(y_0)]\}. \tag{A56b}$$

Since $K_{2/3}(y_0)<K_{5/3}(y_0)$, it is easy to show that

$$0\leq Q(y)\leq\tfrac{5}{3}, \tag{A56c}$$

and this establishes the lemma.

Now inserting (A54) into (A52c), and again applying the mean value theorem, we find

$$\xi_2(\Upsilon)\leq\tfrac{5}{3}\bar{\tau}(1+p\bar{\tau})\xi(\Upsilon),$$

where

$$0\leq\bar{\tau}\leq\tfrac{3}{4}\Upsilon. \tag{A57}$$

This estimate, together with the previous results, implies that (A52a) may be rewritten in the form

$$\xi(\Upsilon)\simeq\tfrac{3}{8}(\Upsilon/p)[1-\Theta(\Upsilon)]^{-1}\times\exp(-8/3\Upsilon)\kappa(\tfrac{3}{4}p\Upsilon), \qquad \Upsilon\ll1; \tag{A58}$$

where the quantity $\Theta(\Upsilon)$ derives from the $\mathcal{O}(\bar{\tau}^2)$ term in (A57). It can easily be verified that $0\leq\Theta(\Upsilon)\leq5/12$; and in the present order of approximation this may be neglected. The bremsstrahlung function appearing in (A58) may be simplified since $\frac{3}{4}p\Upsilon\gg1$, and one of the asymptotic expansions of (2.12) can be used. The corresponding estimate for $\Xi(\Upsilon)$ can then be written as

$$\Xi(\Upsilon)\simeq0.4\Upsilon^{1/2}\exp(-10/3\Upsilon), \qquad \Upsilon\ll1. \tag{A59}$$

REFERENCES

A1 Amaldi, E., *et al.* CERN Rept. 63-13, p. 5.
A2 Arzimovich, L., and I. Pomeranchuk, J. Phys. USSR **9,** 267 (1945).
A3 Alekseev, A. I., Zh. Eksperim. i Teor. Fiz. **31,** 909 (1956) [English transl.: Soviet Phys.—JETP **4,** 771 (1957)].
A4 Aditya, P. K., Nuovo Cimento **11,** 546 (1959).
B1 Beck, F., H. Steinwedel, and G. Sussman, Z. Physik **171,** 189 (1963).
B2 Blewett, J. P., Phys. Rev. **69,** 87 (1946).
B3 Barrat, J. P., Ph.D. dissertation, Université de Paris (1959).
B4 Barrat, J. P., J. Physique **20,** 541 (1959).
B5 Badalyan, A. M., and Ya. A. Smorodinskii, Zh. Eksperim. i Teor. Fiz. **40,** 1231 (1961) [English transl.: Soviet Phys.—JETP **13,** 865 (1961)].
B6 Bhabha, H. J., Proc. Roy. Soc. (London) **A152,** 559 (1935).
B7 Block, M. M., and D. T. King, Phys. Rev. **95,** 171 (1954).
B8 Bolsterli, M., Phys. Rev. **94,** 367 (1954).
C1 Caird, R. S., W. B. Garn, D. B. Thomson, and C. M. Fowler, J. Appl. Phys. **35,** 781 (1964).
C2 Carleman, T., *Les fonctions quasi-analytiques* (Herman et Cie., Paris, 1926).
C3 Criegee, L., Z. Physik **158,** 433 (1960).
D1 Demeur, M., Acad. Roy. Belg. Cl. Sci. Mem. Coll. **28,** No. 5 (1953).
D2 Dovzhenko, O. I., and A. A. Pomanskii, Zh. Eksperim. i Teor. Fiz. **45,** 268 (1963) [English transl.: Soviet Phys.—JETP **18,** 187 (1964)].
D3 Davies, H., H. A. Bethe, and L. C. Maximon, Phys. Rev. **93,** 788 (1954).
E1 Erber, T., Nature **190,** 25 (1961).
E2 Erber, T., in *High Magnetic Fields,* edited by H. Kolm *et al.* (Technology Press, Cambridge, Mass., 1962), p. 706.
E3 Erber, T., and H. C. Shih, Acta Phys. Austriaca **19,** 17 (1964).
E4 Erber, T., Fortschr. Phys. **9,** 343 (1961).
E5 Erber, T., and H. C. Shih, in *Proceedings of the Conference on the Role of Atomic Electrons in Nuclear Transformations* (Polish Academy of Sciences, Warsaw, 1965), Vol. 3, p. 520.
E6 Erber, T., Ann. Phys. (N.Y.) **8,** 435 (1959).
E7 Erber, T., Bull. Am. Phys. Soc. **10,** 536 (1965).
E8 Ehlotzky, F., Acta Phys. Austriaca **18,** 266 (1964).
E9 Euler, H., Ann. Physik **26,** 398 (1936).
E10 Erber, T., and A. Gordon, Math. Computation **17,** 162 (1963).
E11 Erber, T., and H. G. Latal, Bull. Am. Phys. Soc. **10,** 1103 (1965).
F1 Fowler, C. M., W. B. Garn, and R. S. Caird, J. Appl. Phys. **31,** 588 (1960).
F2 Fowler, C. M., R. S. Caird, W. B. Garn, and D. B. Thomson in *High Magnetic Fields,* edited by H. Kolm *et al.* (Technology Press, Cambridge, Mass., 1962), p. 269.
F3 Furry, W. H., Phys. Rev. **51,** 125 (1937).
F4 Furry, W. H., Phys. Rev. **81,** 115 (1951).
F5 Feinberg, E. L., and I. Pomeranchuk, Suppl. Nuovo Cimento **3,** 652 (1956).
F6 Frisch, O. R., Acta Phys. Austriaca **12,** 331 (1959).
F7 Fermi, E., Z. Physik **29,** 315 (1924).
G1 Galitsky, V. M., and I. I. Gurevitch, Nuovo Cimento **32,** 396 (1964).
G2 Galitsky, V. M., and V. V. Yakimets, Zh. Eksperim. i Teor. Fiz. **46,** 1066 (1964) [English transl.: Soviet Phys.—JETP **19,** 723 (1964)].
G3 Guzenko, S. Ya., and P. I. Fomin, Zh. Eksperim. i Teor. Fiz. **47,** 2276 (1964) [English transl.: Soviet Phys.—JETP **20,** 1523 (1965)].
H1 Heitler, W., *Quantum Theory of Radiation* (Clarendon Press, Oxford, England, 1954), 3rd ed., p. 337.
H2 Heisenberg, W., and H. Euler, Z. Physik **98,** 714 (1935).
I1 Iwanenko, D., and I. Pomeranchuk, Phys. Rev. **65,** 343 (1944).
J1 Jauch, J. M., and K. M. Watson, Phys. Rev. **74,** 950 (1948); **74,** 1485 (1948).
J2 Johnson, M. H., and B. A. Lippmann, Phys. Rev. **76,** 828 (1949).
K1 Kaitna, R., Ph.D. dissertation, Universität Graz (1963).
K2 Kaitna, R., and P. Urban, Nucl. Phys. **56,** 518 (1964).
K3 Källén, A. O. G., *Handbuch der Physik,* S. Flügge, Ed. (Springer-Verlag, Berlin, 1958), Vol. 5, Part 1.
K4 Klepikov, N. P., Zh. Eksperim. i Teor. Fiz. **26,** 19 (1954).
K5 Klepikov, N. P., Ph.D. thesis, University of Moscow (1952).

K6 Koch, H. W., and J. W. Motz, Rev. Mod. Phys. **31,** 920 (1959).

K7 Kuraev, E. A., and S. S. Sannikov, Zh. Eksperim. i Teor. Fiz. **44,** 1015 (1963) [English transl.: Soviet Phys.—JETP **17,** 688 (1963)].

K8 Katz, L., and K. H. Lokan, Nucl. Instr. Methods **11,** 7 (1961).

L1 Landau, L. D., and E. M. Lifshitz, *The Classical Theory Fields* (Pergamon Press, Oxford, England, 1962), revised second edition, p. 235.

L2 Lerch, M., Acta Math. **27,** 339 (1903).

L3 Landau, L., and I. Pomeranchuk, Doklady Akad. Nauk SSSR **92,** 535, 735 (1953).

L4 Lutzky, M., and J. S. Toll, Phys. Rev. **113,** 1649 (1959).

M1 Malkus, W. V. R., Phys. Rev. **83,** 899 (1951).

M2 Mark, H., Nucl. Instr. Methods **28,** 131 (1964).

M3 Migdal, A. B., Phys. Rev. **103,** 1811 (1956).

M4 Migdal, A. B., Zh. Eksperim. i Teor. Fiz. **32,** 633 (1957).

M5 Murota, T., A. Ueda, and H. Tanaka, Progr. Theoret. Phys. **16,** 482 (1956).

N1 Neuman, M., Phys. Rev. **90,** 682 (1953).

P1 Pomeranchuk, I., J. Phys. (USSR) **2,** 65 (1940).

R1 Robl, H., Acta Phys. Austriaca **6,** 45 (1952).

R2 Robl, H., Acta Phys. Austriaca **6,** 105 (1952).

S1 Schiff, L. I., Am. J. Phys. **20,** 474 (1952).

S2 Schwinger, J., Phys. Rev. **75,** 1912 (1949).

S3 Schott, G. A., *Electromagnetic Radiation* (Cambridge University Press, Cambridge, England, 1912).

S4 Schwinger, J., Phys. Rev. **75,** 898 (1949).

S5 Smith, F. T., Phys. Rev. **118,** 349 (1960).

S6 Sannikov, S. S., Zh. Eksperim. i Teor. Fiz. **42,** 282 (1962) [English transl.: Soviet Phys.—JETP **15,** 196 (1962)].

S7 Synge, J. L., *Principal Null Directions Defined in Space Time by an Electromagnetic Field* (University of Toronto Press, Toronto, 1935), Appl. Math. Ser. No. 1.

S8 Schrödinger, E., Proc. Roy. Irish Acad. **A47,** 77 (1942).

S9 Skobov, V. G., Zh. Eksperim. i Teor. Fiz. **35,** 1315 (1958) [English transl.: Soviet Phys.—JETP **8,** 919 (1959)].

S10 Sakharov, A. D., *et al.*, Dokl. Akad. Nauk SSSR **165,** 65 (1965) [English transl.: Soviet Phys.—Doklady **10,** 1045 (1966)].

T1 Toll, J., Ph.D. dissertation, Princeton University (1952).

T2 Ter-Mikaeljan, M. L., Doklady Akad. Nauk SSSR **94,** 1033 (1954).

T3 Toptygin, I. N., Zh. Eksperim. i Teor. Fiz. **46,** 851 (1964) [English transl.: Soviet Phys.—JETP **19,** 583 (1964)].

T4 Tomonaga, S., and M. Kobayasi, Sci. Papers Inst. Phys. Chem. Res. (Tokyo) **34,** 1643 (1938).

U1 Überall, H., Phys. Rev. **103,** 1055 (1956).

W1 Watson, G. N., *Bessel Functions* (Cambridge University Press, Cambridge, England, 1952).

W2 Wall, H. S., *Analytic Theory of Continued Fractions* (D. Van Nostrand Co., Inc., New York, 1948), pp. 327–330.

W3 Weizsäcker, C. F., Z. Physik **88,** 612 (1934).

W4 Williams, E. J., Kgl. Danske Videnskab. Selskab, Mat.-Fyz. Medd. **13,** No. 4 (1935).